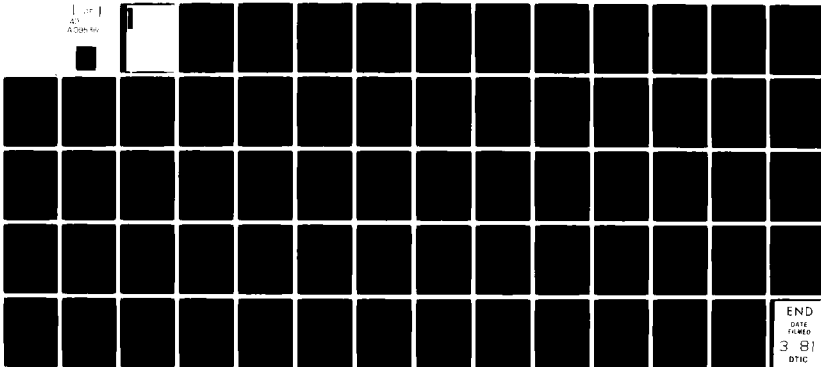


AD-A095 360

NAVAL RESEARCH LAB WASHINGTON DC F/G 9/1
SELF-CONSISTENT NONLINEAR SLOW-TIME SCALE FORMULATION AND SIMUL--ETC(U)
FEB 81 J L VOMVORIDIS, P SPRANGLE
NRL-MR-4426 NL

UNCLASSIFIED

[]
43
AD-66



END
DATE
FILMED
3 81
DTIC

AD A095360

14' NRL-MR-4426

9 REPORT DOCUMENTATION PAGE		READ INSTRUCTIONS BEFORE COMPLETING FORM	
1. REPORT NUMBER NRL Memorandum Report 4261	2. GOVT ACCESSION NO. AD-A095360	3. RECIPIENT'S CATALOG NUMBER	
6 TITLE (and Subtitle) SELF-CONSISTENT NONLINEAR SLOW-TIME SCALE FORMULATION AND SIMULATION OF OVERMODDED GYROTRON OSCILLATORS AND AMPLIFIERS		5. TYPE OF REPORT & PERIOD COVERED Interim report on a continuing NRL problem.	
7. AUTHOR(s) 10 J. L. Vomvoridis* and P. Sprangle		6. PERFORMING ORG. REPORT NUMBER	
9. PERFORMING ORGANIZATION NAME AND ADDRESS Naval Research Laboratory Washington, DC 20375		8. CONTRACT OR GRANT NUMBER(s)	
11. CONTROLLING OFFICE NAME AND ADDRESS Office of Naval Research Arlington, VA 22209		10. PROGRAM ELEMENT, PROJECT, TASK AREA & WORK UNIT NUMBERS 61153N-11 RR0110941 67-0865-0-1, 67-0899-0-1	
14. MONITORING AGENCY NAME & ADDRESS (if different from Controlling Office) 16 RR01109		12. REPORT DATE February 1981	
		13. NUMBER OF PAGES 67	
		15. SECURITY CLASS. (of this report) UNCLASSIFIED	
		15a. DECLASSIFICATION/DOWNGRADING SCHEDULE	
16. DISTRIBUTION STATEMENT (of this Report) Approved for public release; distribution unlimited.			
17. DISTRIBUTION STATEMENT (of the abstract entered in Block 20, if different from Report)			
18. SUPPLEMENTARY NOTES *Present address: JAYCOR, Alexandria, VA 22304			
19. KEY WORDS (Continue on reverse side if necessary and identify by block number) Electron cyclotron maser (Gyrotron) Eigenmode competition Non-linear particle dynamics Slow-time-scale simulations Axial nonuniformities			
20. ABSTRACT (Continue on reverse side if necessary and identify by block number) The gyrotron (or, electron cyclotron maser) operates on the interaction of a TE cavity mode with the relativistic electron cyclotron beam mode. This instability has been seen both theoretically and experimentally to be a very efficient source for microwave generation, useful for the heating of tokamak plasmas at the electron cyclotron frequency. The next generation of tokamaks involves high confining fields and accordingly the gyrotron must produce short (~2mm) wavelength radiation, which can be realized only by a highly overmoded operation of the gyrotron. This work presents the groundwork for the study of such an overmoded operation.			

(Continues)

251950

20. Abstract (Continued)

The self-consistent nonlinear equations have been obtained for the evolution of the electron distribution and of the power spectrum for multimode gyrotron interactions in a rectangular cavity or waveguide. The time step of the resulting algorithm is limited only by the nonlinearities and nonuniformities, and therefore yields very efficient simulations. The equations have been applied to the following cases: (a) in a waveguide, analytically, to obtain the dispersion relation and saturation behavior of a monochromatic wave with two-dimensional transverse structure; (b) in a waveguide, numerically, to test the correctness and accuracy of the computer code; (c) in a waveguide with external field (or equivalent) nonuniformities, to interpret the associated efficiency enhancement; and (d) in a two-mode cavity, to study the evolution and saturation of the eigenmodes.

CONTENTS

LIST OF FIGURES AND TABLES	iv
1. INTRODUCTION	1
2. DEFINITIONS	4
3. THEORETICAL METHOD	10
4. SLOW-TIME SCALE EQUATIONS	14
5. ANALYTICAL APPLICATION IN A WAVEGUIDE	19
6. NUMERICAL APPLICATION IN A WAVEGUIDE	25
7. EFFECTS OF AN EXTERNAL FIELD NONUNIFORMITY	30
8. APPLICATION TO AN OVERMODED CAVITY	39
9. DISCUSSION	48
ACKNOWLEDGMENTS	53
REFERENCES	54

Accession For	
NTIS GRAM	<input checked="" type="checkbox"/>
DTIC	<input type="checkbox"/>
University	<input type="checkbox"/>
Justice	<input type="checkbox"/>
By	
Distribution/	
Availability Codes	
Dist	A, all and/or Special
A	

LIST OF FIGURES

1 — Geometry of the rectangular cavity	5
2 — Definition of transverse position and velocity coordinates	7
3 — Schematic representation of the motion of the bunch	23
4 — Evolution of the average relative phase of the bunch and associated evolution of the growth rate and frequency shift during a bounce period	24
5 — Evolution of (a) the amplitude and (b) the growth rate and the frequency shift for the reference simulation	26
6 — Dependence of growth rate, frequency shift and bounce frequency at saturation on the sharpness of synchronism: Comparison of the simulations to theory	29
7 — Comparison of the trajectories of particles in close resonance with a wave in (a) a uniform medium, to (b) a nonuniform medium, $R \neq 0$. The horizontal line denotes the initial conditions of the beam	32
8 — Schematic representation for the evolution of the bunch for a nonuniform external field, (a) when $R > 0$, $\theta_{+0} \gtrsim 2\omega_b(1-R)$, and (b) when $R < 0$, $\theta_{+0} \lesssim 2\omega_b(1+R)$	35
9 — Schematic representation for the evolution of a beam with temperature, (a) when $R > 0$, with no particles initially trapped, and (b) when $R < 0$, with the trapping region initially filled	37
10 — Evolution of the (a) amplitude and (b) frequency of the resonant modes for case 4 of Table 2. The horizontal broken lines in (b) give the empty cavity frequencies ..	43
11 — Relative phase of mode 1 to mode 2, $\phi_1 - \phi_2$, versus time for the simulation of Fig. 10	46

LIST OF TABLES

1 — Dependence of Γ , Δ and Ω_{\max} on the input parameters for applications in a waveguide	28
2 — Characteristics of the evolution of the dominant mode in a two-mode cavity with $Q_1 = 1000$ and $Q_2 = 700$. The modes denoted by an asterisk have been primed ...	41

SELF-CONSISTENT NONLINEAR SLOW-TIME SCALE FORMULATION AND SIMULATION OF
OVERMODED GYROTRON OSCILLATORS AND AMPLIFIERS

1. INTRODUCTION

The gyrotron (or, electron cyclotron maser) instability arises from the interaction of a TE waveguide (or cavity) mode with a relativistic electron beam, which drifts along and rotates about an externally applied static magnetic field. This instability occurs for sufficiently close synchronization of the relativistic electron gyrofrequency in the external field to the wave frequency, Doppler shifted in the electron frame, since it is then that the wave electric field acts on the beam electrons coherently, causing changes in their relativistic factor, γ , depending on the electron phase relative to the wave, resulting in phase slippage and bunching, with the corresponding current driving in turn the wave. Voluminous theoretical and experimental investigations of this instability (1-12 and references therein) have established the gyrotron as a very potent source for microwave generation, with inherent efficiencies approaching 50%. Further improvements to this value for the efficiency are possible by introducing axial gradients either in the diameter of the oscillator (13, 14), hence the axial wavenumber, or in the guiding field (15-17).

In view of the impressive performance of the gyrotron in converting the kinetic energy of the beam electrons to electromagnetic energy, it is the prime candidate to be used as the radiation source for the heating of tokamak plasmas at the electron cyclotron frequency. For the parameters

Manuscript submitted December 4, 1980.

currently considered, e.g., for a confining field of the order of 50 kG, requiring a radiation wavelength of the order of 2 mm, the obvious size and power limitations require an operation of the gyrotron not at the fundamental harmonic. Accordingly, it is required that the operation of an overmoded gyrotron cavity be investigated, to assess the performance of the desired mode and the potential of destructive interference by the competing modes.

The problem of multimode interactions in an electron cyclotron maser has been addressed analytically in the Soviet literature (19-20). In their analysis, the coupled system of equations for the eigenmodes and the beam distribution is presented, and the coupling coefficients are expressed in terms of series involving the even powers of the field amplitudes. From the consideration of the coefficients of these expansions, distinction between soft and hard coupling is made and general conditions are given to distinguish between stable and unstable equilibria. This approach is mathematically involved to an extent that obscures the physics of the interaction, and its applicability appears limited to situations involving restrictions, such as, a low amplitude for all but one mode, or small beat frequencies compared to the inverse of the electron transit time through the resonator, or a premodulated electron beam, or an identical axial dependence of the modes.

An alternate approach has been recently initiated at NRL (21), in which the motion of test particles is followed in cavity waves with constant amplitude and frequency, the latter taken equal to the empty cavity eigenfrequency. Equating the energy lost by the particles to each mode to the diffraction losses gives the values of the quality factors, Q , consistent

with equilibrium, and, by iteration, the equilibrium amplitudes (and efficiencies) for given values of Q (and of the beam power). A presentation of these results in the form of contour plots appears to be very useful for the determination of the operating conditions. However, these results are liable to reservations regarding the assumption of constant (and not oscillating at the beat frequency) amplitudes and frequencies, and that the latter is not shifted by the action of the beam.

The purpose of this work has been to develop and apply a self-consistent formulation for the multi-mode problem, which is simultaneously adoptable for efficient numerical simulations and applicable for theoretical considerations. After a brief description of the physical model in Sec. 2, the theoretical method is discussed in Sec. 3, while the resulting equations are presented in Sec. 4, along with a discussion on the algebraic manipulations that led to their derivation. In order to establish the correctness of the equations and to demonstrate their applicability for an analytical treatment, they are used in Sec. 5 to rederive and generalize the equations pertinent to the evolution in a waveguide, and this evolution is shown in Sec. 6 to be accurately described by the algorithm based on these equations. Some consideration of introductory nature is given in Sec. 7, on the interaction responsible for the efficiency enhancement in a nonuniform external field, while examples on the application to an overmoded cavity are presented in Sec. 8. Finally Sec. 9 summarizes our results, compares our method to the test particle approach, and indicates various possible extensions to this work.

2. DEFINITIONS

This section serves the purpose of defining the physical model we are considering and the nomenclature for the quantities of interest.

We consider a rectangular cavity with perfectly conducting walls. The transverse dimensions of the cavity are x_{\max} and y_{\max} , and the length is z_{\max} (Fig. 1). The choice of the rectangular geometry was for the purpose of simplifying the algebra, while the physics of the interaction is not obscured. The results obtained with this geometry can be directly applied to a coaxial cavity with large aspect ratio, while for a general cylindrical geometry an appropriate conversion of either the results or the formalism is necessary.

An external magnetic field is present inside the cavity. The main component of this field is $B_z^{(ex)}$, along the axis of the cavity, however, a weak nonuniformity is allowed, i.e., $\partial B_z^{(ex)}/\partial z$ and the transverse components, $B_x^{(ex)}$ and $B_y^{(ex)}$, are small but not necessarily zero. The introduction of this nonuniformity is for the purpose of assessing the associated efficiency enhancement (15, 16), similar to the corresponding behavior in the case of the Whistler mode (22, 23). For normalization purposes, it is appropriate to express the external field components by their nonrelativistic electron gyrofrequencies, Ω_x , Ω_y and Ω_z , defined by $\Omega_z = eB_z^{(ex)}/m_e c$, with similar definitions for Ω_x and Ω_y , where $-e$ and m_e are the electron charge and rest mass, respectively, while c is the speed of light.

An electron beam is continuously injected into the cavity at $z = 0$ and propagates self-consistently with the external magnetic field and the cavity fields, defined below. The distribution function of the electrons is defined as

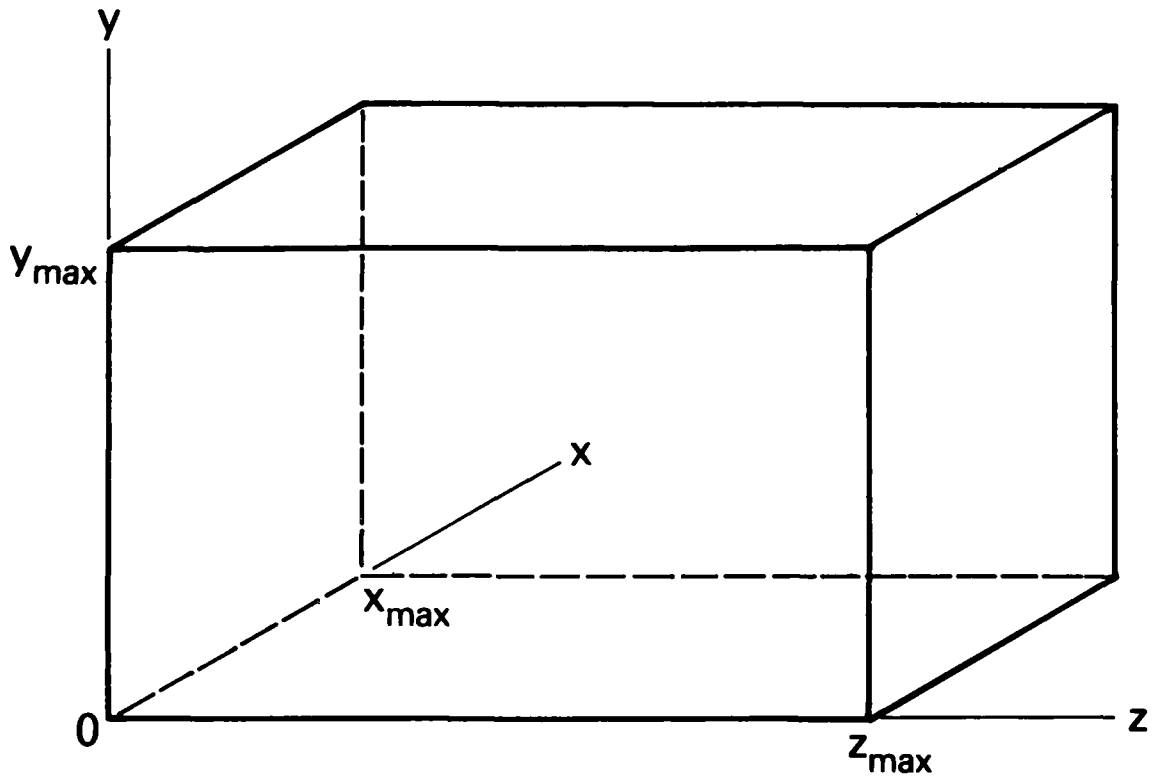


Fig. 1 - Geometry of the rectangular cavity.

$$f(\underline{r}, \underline{v}, t) = \sum_{i=1}^{i_{\max}(t)} \delta(\underline{v} - \underline{v}_i(t)) \delta(\underline{r} - \underline{r}_i(t)), \quad (1)$$

where $\underline{r}_i(t)$ and $\underline{v}_i(t)$ are the instantaneous position and velocity vectors of the i -th particle, obtained from its equations of motion in terms of its entry properties, and $i_{\max}(t)$ is the number of particles inside the cavity at time t . No assumption is made with regard to the form of the distribution function at $z = 0$, hence it is possible to consider the effect associated with a position or velocity spread of the electrons or with any slow time dependence of their bulk entry properties (e.g., velocity or density). It is convenient to introduce the instantaneous plasma frequency, $\omega_p(t)$, of the beam, defined by $\omega_p^2 = (4\pi e^2 i_{\max}) / (m_e x_{\max} y_{\max} z_{\max})$. It is assumed that the beam density and axial velocity inside the cavity are not too much different from those outside, so that any effects on the beam distribution by its self-fields can be adequately accounted for by an appropriate expression of the distribution function at the entry point. However, the exact (i.e., self-consistent) particle density and axial velocities inside the cavity will be considered for the computation of the beam effect on the cavity fields. The transverse components of the position, (x, y) , and velocity (v_x, v_y) , of the electrons are expressed by the position of the guiding center, (\bar{x}, \bar{y}) , and the amplitude and phase of the velocity, (v_{\perp}, ψ) , defined by

$$\begin{aligned} x &= \bar{x} + \rho \sin \psi, & y &= \bar{y} - \rho \cos \psi, \\ v_x &= v_{\perp} \cos \psi, & v_y &= v_{\perp} \sin \psi, \end{aligned} \quad (2)$$

as shown in Fig. 2, where $\rho = \gamma v_{\perp} / \Omega_z$ is the Larmor radius and $\gamma = c / (c^2 - v_z^2 - v_{\perp}^2)^{1/2}$ is the relativistic factor. Obviously, this transformation is suggested by the fact that the principal motion of the electrons

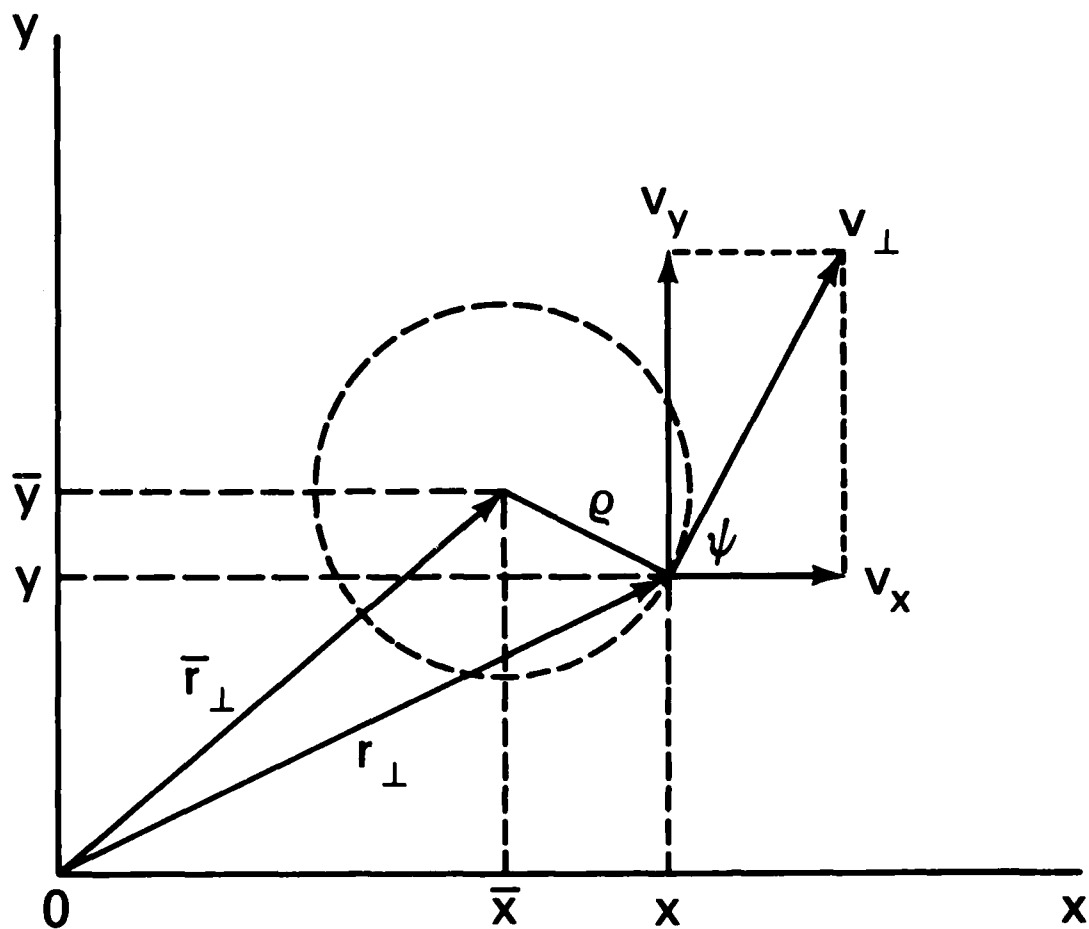


Fig. 2 - Definition of transverse position and velocity coordinates.

is that under the action of the axial external field component, $B_z^{(ex)}$.

The fields of the cavity are expanded in terms of the vacuum eigenmodes. Since the gyrotron instability involves the TE modes, only these modes are included in the expansion. The (n, m, ℓ) mode is characterized by the constant wavenumbers (k_n, k_m, k_ℓ) corresponding to the three Cartesian axes and defined by $k_n = n\pi/x_{\max}$ ($n = 0, 1, 2, \dots$), $k_m = m\pi/y_{\max}$ ($m = 0, 1, 2, \dots$) with the restriction $n + m \neq 0$, and $k_\ell = \ell\pi/z_{\max}$ ($\ell = 1, 2, 3, \dots$). The transverse wavenumber is defined by $k_{nm} = (k_n^2 + k_m^2)^{1/2}$ and the total wavenumber is $k_{nm\ell} = (k_{nm}^2 + k_\ell^2)^{1/2}$. The time evolution of each mode is described by the variation of the amplitude, $B_{nm\ell}(t)$, or its electron gyrofrequency, $\Omega_{nm\ell} = eB_{nm\ell}/mc$, and the phase, $\phi_{nm\ell}(t)$, or the frequency, $\omega_{nm\ell} = d\phi_{nm\ell}/dt$. In addition, we use the growth rate, $\Gamma_{nm\ell} = \Omega_{nm\ell}^{-1} d\Omega_{nm\ell}/dt$, and the frequency shift, $\Delta_{nm\ell} = \omega_{nm\ell} - k_{nm\ell} c$, as well as the quality factor, $Q_{nm\ell}$, which is assumed to be much larger than unity. Using the above definitions and the shorthand notations $C_n = \cos(k_n x)$, $S_n = \sin(k_n x)$, $C_m = \cos(k_m y)$, $S_m = \sin(k_m y)$, $C_\ell = \cos(k_\ell z)$ and $S_\ell = \sin(k_\ell z)$, the cavity fields are given by

$$B_z^{(w)} = \sum_{nm\ell} C_n C_m S_\ell B_{nm\ell} \sin \phi_{nm\ell} ,$$

$$B_x^{(w)} = - \sum_{nm\ell} \frac{k_n k_\ell}{k_{nm}^2} S_n C_m C_\ell B_{nm\ell} \sin \phi_{nm\ell} ,$$

$$B_y^{(w)} = - \sum_{nm\ell} \frac{k_m k_\ell}{k_{nm}^2} C_n S_m C_\ell B_{nm\ell} \sin \phi_{nm\ell} ,$$

$$E_z^{(w)} = 0 ,$$

$$E_x^{(w)} = \sum_{nm\ell} \frac{k_m}{ck_{nm}^2} C_n S_m S_\ell \frac{d}{dt} (B_{nm\ell} \sin \phi_{nm\ell}) ,$$

(3)

$$E_y^{(w)} = - \sum_{nm\ell} \frac{k_n}{ck_{nm}^2} S_n C_m S_\ell \frac{d}{dt} (B_{nm\ell} \sin \phi_{nm\ell}),$$

for the components of the magnetic induction and electric field along the z, x and y axes, respectively. The summation formally extends over the triple infinity of eigenmodes supported by the cavity, however, when our resultant equations are to be used, it suffices to sum only over those modes whose forward or backward component is adequately resonant with the beam.

The quantity of interest in oscillators is the efficiency, $\eta_{nm\ell}$, of conversion of beam power to radiation power of the mode (n, m, ℓ). Calculating the field energy from Eq. (3), multiplying by $\omega_{nm\ell}/Q_{nm\ell}$ and dividing the result, the radiation power, by the beam power yields the formula for the efficiency,

$$\eta_{nm\ell} = \frac{1 + \delta_{nm,0}}{16} \frac{\omega_{nm\ell} z_{\max}}{(\gamma_0 - 1) v_{z0} Q_{nm\ell}} \left(\frac{\omega_{nm\ell}}{k_{nm} c} \right)^2 \left(\frac{\Omega_{nm\ell}}{\omega_{p0}} \right)^2, \quad (4)$$

where $\delta_{nm,0} = 1$, if either $n = 0$ or $m = 0$, and $\delta_{nm,0} = 0$, otherwise. The efficiency in Eq. (4) is calculated in terms of the instantaneous values of $\omega_{nm\ell}$ and $\Omega_{nm\ell}$ and the entry values γ_0 , v_{z0} and ω_{p0} of the beam, which may be slowly time dependent, if a beam with variable properties is employed.

3. THEORETICAL METHOD

In principle, the solution to the problem involves the solution of the wave equation for the cavity fields, e.g.,

$$(\nabla^2 - \frac{1}{c^2} \frac{\partial^2}{\partial t^2}) \underline{B}^{(w)} = - \frac{4\pi}{c} (\underline{\nabla} \times \underline{J}) \quad , \quad (5a)$$

with the current density, $\underline{J}(\underline{r}, t) = - e \int d\underline{v} \underline{v} f(\underline{r}, \underline{v}, t)$, obtained from the solution of the equations

$$\frac{d}{dt} \underline{r} = \underline{v} \quad , \quad (5b)$$

$$\frac{d}{dt} (\gamma \underline{v}) = - \frac{e}{mc} \left[c \underline{E}^{(w)} + \underline{v} \times (\underline{B}^{(w)} + \underline{B}^{(ex)}) \right] \quad ,$$

for the relativistic motion of the beam electron under the joint action of the cavity and external fields. The above equations, together with Faraday's law, $c \underline{\nabla} \times \underline{E}^{(w)} + \partial \underline{B}^{(w)} / \partial t$, form a complete system, whose solution can be Fourier analyzed in the eigenmodes, Eq. (3), to give the evolution of the spectrum. Such an approach, although straightforward conceptually, has limitations associated with its numerical implementation, since it involves a large number of arithmetic operations. In addition, for a theoretical investigation of the physics of the multi-mode interaction, this approach is not useful, since its equations are not formulated in the time scale of the energy transfer from the beam electrons to the fields.

The aim of this work is to develop a formulation which is both efficient for numerical applications and useful for theoretical considerations, without sacrificing the rigor of self-consistency. The central assumption in our approach is that there exists a time interval, Δt , during which the energy

transfer between the electrons and the fields, and between the parallel and perpendicular components of the electron motion, is small, while Δt is not necessarily small compared to the gyroperiod or the wave period. For a numerical application of our equations, Δt will be the time step. Then, according to our assumption, the quantities $\omega_{nm\ell}$, $\Omega_{nm\ell}$, \bar{x}_i , \bar{y}_i , $v_{\perp i}$ and v_{zi} will be constant to zero order during the time interval Δt , while the quantities $\phi_{nm\ell}$, z_i and ψ_i will vary linearly with time,

$$\phi_{nm\ell}(t) = \phi_{nm\ell}(t_0) + (t - t_0) \omega_{nm\ell}(t_0) ,$$

$$z_i(t) = z_i(t_0) + (t - t_0) v_{zi}(t_0) , \quad (6)$$

$$\psi_i(t) = \psi_i(t_0) + (t - t_0) \Omega_z(z_i(t_0)) / \gamma_i(t_0) ,$$

where t_0 is the time at the beginning of the time step and $t - t_0 \leq \Delta t$. These zero order solutions can be introduced into the differential equations to obtain the first order equations for the electron propagation and wave evolution at the time scale of energy transfer.

Formally, the above assumption can be described quantitatively by the strong inequality

$$\omega, kc, \Omega_z \gg \Gamma, \Delta, \theta_{\pm}, \frac{\omega}{Q}, \Omega, \Omega_x, \Omega_y, \frac{1}{k_{\ell}} \frac{\partial \Omega_z}{\partial z} , \quad (7)$$

where the subscript triad $nm\ell$ has been suppressed and $\theta_{\pm} = \theta_{\pm nm\ell, i} = \Omega_z / \gamma_i - \omega_{nm\ell} \pm k_{\ell} v_{zi}$ is the rate of change of the particle phase, ψ_i , relative to the wave phase in the particle rest frame, $\phi_{nm\ell} \pm k_{\ell} z_i$. Using this inequality,

each quantity of interest, say q , where q stands for \bar{x} , \bar{y} , z , v_x , v_z , ψ , Γ and Δ or any combination of them (like γ), can be associated with a differential equation, which is expanded in the form

$$\frac{dq}{dt} = A_{00} + \sum_{i=1}^{\infty} \sum_{j=0}^{\infty} A_{ij} \sin(\alpha_j t + p_j) \quad , \quad (8)$$

where the amplitudes are required to satisfy $A_{ij} \gg A_{i+1,j}$ and $A_{ij} \sim A_{i,j+1}$, and the frequencies $\alpha_j \ll \alpha_{j+1}$, with p_j being an appropriate phase. The quantities A_{ij} , α_{ij} and p_j are assumed to vary slowly during the energy transfer time, i.e., to be constant during Δt . The zero order term, A_{00} , represents the unperturbed cyclotron motion of the electrons in a uniform external field and the steady state propagation of the cavity modes, while the terms under the summation represent the effects to first and higher order (given by i) of the nonuniformity and of wave-particle coupling, and the slow ($j=0$) and fast (to all degrees, j) phase variations. The slowest phase variation corresponds to guiding center motion in the nonuniform external field ($\alpha_0 = 0$) and to resonant interaction, $\alpha_0 = \theta_{\pm}$.

Clearly, there is no need to evaluate and use many terms in the expansion of Eq. (8). A truncation,

$$\frac{dq}{dt} = A_{00} + A_{10} \sin(\alpha_0 t + p_0) \quad , \quad (9)$$

is expected to be sufficient, since the contribution of the higher order terms, $i > 1$, is negligible, $(A_{ij}/A_{00}) \sim (A_{10}/A_{00})^i \ll 1$, and the effects of the fast terms, $j > 0$, phase mixes to zero during the energy transfer time, in view of

$\alpha_j/\Gamma \sim j\omega/\Gamma \gg 1$. In this sense, our approach is conceptually identical to that already employed for electrostatic and whistler waves (24).

A final remark is associated with the choice of time, t , rather than the axial position, z , as independent variable. Certainly, the conversion of the method and the equations is straightforward, by the simple transformation $dt = dz/v_z$. The reason behind this choice has been to guard against the possibility that the parameters of some electrons become multi-valued functions of z , which could well be the case especially due to the nonuniformity, and to avoid complications in the evaluation of the wave properties, which are necessarily time dependent quantities and would be obtainable by an appropriate interpolation in the electron dynamics.

4. SLOW-TIME-SCALE EQUATIONS

In this section we present the slow-time-scale equations for the propagation of the electrons and the evolution of the eigenmodes. Our approach has already been discussed in the previous section. Since the procedure involves a lengthy series of calculations which, however, are of elementary nature, we will limit ourselves to the presentation of the final results, with only a discussion of the steps used in obtaining them. (See also Ref. 25.)

The slow-time-scale equations for the electron dynamics are:

$$\begin{aligned}
 \frac{d}{dt} (\gamma v_z) &= -\frac{1}{2} v_{\perp}^2 \frac{\partial \bar{\Omega}_z}{\partial z} \\
 &\quad - \frac{1}{2} \sum_{nm\ell} \left[J_1' \frac{k_{\perp} v_{\perp} \Omega_{nm\ell}}{k_{nm}^2} \sum_{\pm} (k_m \bar{c}_n \bar{s}_m \sin \zeta_{\pm} + k_n \bar{s}_n \bar{c}_m \cos \zeta_{\pm}) \right], \\
 \frac{d}{dt} (\gamma v_{\perp}) &= \frac{1}{2} v_z^2 \frac{\partial \bar{\Omega}_z}{\partial z} \\
 &\quad - \frac{1}{2} \sum_{nm\ell} \left[J_1' \frac{\bar{\Omega}_z \Omega_{nm\ell}}{\gamma k_{nm}^2} \sum_{\pm} \left(1 - \frac{\gamma \theta_{\pm}}{\bar{\Omega}_z} \right) (k_m \bar{c}_n \bar{s}_m \sin \zeta_{\pm} + k_n \bar{s}_n \bar{c}_m \cos \zeta_{\pm}) \right] \\
 \frac{d}{dt} \gamma &= -\frac{1}{2} \sum_{nm\ell} \left[J_1' \frac{\omega_{nm\ell} v_{\perp} \Omega_{nm\ell}}{k_{nm}^2 c^2} \sum_{\pm} (k_m \bar{c}_n \bar{s}_m \sin \zeta_{\pm} + k_n \bar{s}_n \bar{c}_m \cos \zeta_{\pm}) \right], \\
 \frac{d}{dt} \psi &= \frac{1}{\gamma} (\bar{\Omega}_z + v_z \frac{\partial \bar{\Omega}_z}{\partial z} \int dt - \frac{\bar{\Omega}_z}{\gamma} \int \frac{d\gamma}{dt} dt) \\
 &\quad + \frac{1}{2} \sum_{nm\ell} \left[J_1' \frac{\Omega_{nm\ell}}{\gamma k_{nm}} \sum_{\pm} (\pm 1) \left(1 - \frac{1 - \gamma \theta_{\pm} / \bar{\Omega}_z}{k_{nm}^2 \rho^2} \right) \right. \\
 &\quad \quad \left. \times (k_m \bar{c}_n \bar{s}_m \cos \zeta_{\pm} - k_n \bar{s}_n \bar{c}_m \sin \zeta_{\pm}) \right], \tag{10}
 \end{aligned}$$

$$\frac{d}{dt} z = v_z \left(1 + \frac{1}{\gamma v_z} \int \frac{d(\gamma v_z)}{dt} dt - \frac{1}{\gamma} \int \frac{dy}{dt} dt \right) ,$$

$$\frac{d}{dt} \bar{x} = \frac{1}{2} \frac{\rho^2}{\gamma} \frac{\partial \bar{\Omega}_z}{\partial y} + \frac{v_z}{\bar{\Omega}_z} \left(\bar{\Omega}_x + v_z \frac{\partial \bar{\Omega}_x}{\partial z} \int dt \right)$$

$$- \frac{1}{2} \sum_{nm\ell} \frac{\Omega_{nm\ell}}{\bar{\Omega}_z k_{nm}^2} \left[J_1' k_m v_\perp \sum_{\pm} (\pm 1) (k_m \bar{C}_n \bar{C}_m \cos \zeta_{\pm} + k_n \bar{S}_n \bar{S}_m \sin \zeta_{\pm}) \right. \\ \left. + J_1 \frac{k_n}{k_{nm}} \sum_{\pm} (\pm \theta_{\pm}) (k_n \bar{C}_n \bar{C}_m \cos \zeta_{\pm} - k_n \bar{S}_n \bar{S}_m \sin \zeta_{\pm}) \right] ,$$

$$\frac{d}{dt} \bar{y} = - \frac{1}{2} \frac{\rho^2}{\gamma} \frac{\partial \bar{\Omega}_z}{\partial x} + \frac{v_z}{\bar{\Omega}_z} \left(\bar{\Omega}_y + v_z \frac{\partial \bar{\Omega}_y}{\partial z} \int dt \right)$$

$$- \frac{1}{2} \sum_{nm\ell} \frac{\Omega_{nm\ell}}{\bar{\Omega}_z k_{nm\ell}} \left[J_1' k_n v_\perp \sum_{\pm} (\pm 1) (k_n \bar{C}_n \bar{C}_m \sin \zeta_{\pm} + k_m \bar{S}_n \bar{S}_m \cos \zeta_{\pm}) \right. \\ \left. + J_1 \frac{k_m}{k_{nm}} \sum_{\pm} (\pm \theta_{\pm}) (k_m \bar{C}_n \bar{C}_m \sin \zeta_{\pm} - k_n \bar{S}_n \bar{S}_m \cos \zeta_{\pm}) \right] .$$

In the above equations, a superscripted bar denotes evaluation at the guiding center, i.e., $\bar{C}_n = \cos(k_n \bar{x})$ etc., J_1 and J_1' are the Bessel function of first kind and first order and its derivative, both evaluated at $k_{nm}\rho$, where $\rho = \gamma v_\perp / \bar{\Omega}_z$ is the Larmor radius, and $\zeta_{\pm} = \psi - \phi_{nm\ell} \pm k_\ell z$ is the electron phase relative to the forward/backward wave and $\theta_{\pm} = d\zeta_{\pm}/dt$ is the corresponding relative frequency. For numerical purposes, these equations can be integrated analytically over the time step, Δt , since during that time all quantities of the right-hand side can be considered to be constant, except for ζ_{\pm} , for which

a variation $d\underline{z}_+/dt = \underline{z}_+(t_0) + (t - t_0) \underline{\theta}_+(t_0)$ is sufficient, in terms of the corresponding values at t_0 , the beginning of the time step. These integrated expressions can be used to evaluate the integrals of $d\underline{\gamma}/dt$ and $d(\underline{\gamma}v_z)/dt$, which appear on the right hand-side of Eq. (10), thus resulting in an algebraic single-step algorithm. Although this algorithm includes linear equations in a uniform external field, a successive application of these equations will give the nonlinear nonuniform final solution, since the nonlinearities and nonuniformities are accounted for by the reinitialization after each time step.

Let us present now a few comments on the derivation of Eq. (10). We have started with the equation of motion, Eq. (5b), in which the external and wave fields are treated separately, the latter expressed by Eq. (3) and the transverse position and velocity are expressed by Eq. (2), resulting in the evaluation of certain quantities of (\bar{x}, \bar{y}) , as indicated in Eq. (10) by the superscripted bars. With regard to the contribution of the cavity fields, expressions similar to $\cos(k_{nm}\rho \cos\psi_1)$ are expanded in Fourier series, with the coefficients obtained from the integral representation of the Bessel functions,

$$J_n(k_{nm}\rho) = \frac{1}{\pi} \int_0^\pi \cos(k_{nm}\rho \sin\psi - n\psi) d\psi, \quad (11)$$

as well as their symmetry relations. The products of trigonometric functions are converted to sums whose argument changes at the frequency $s\Omega_z/\gamma \pm \omega \pm k_\rho v_z$. We consider only interactions at the fundamental ($s=1$) and elimination of the fast terms, $\Omega_z/\gamma + \omega \pm k_\rho v_z$, leaves only the two slow relative frequencies, $\underline{\theta}_+$, and the corresponding phase angles, \underline{z}_+ , in terms of which Eq. (10) is expressed. A similar application of Eqs. (5) and (2) on the external field contribution, in which terms varying at the frequencies Ω_z/γ and $2\Omega_z/\gamma$ are

omitted, gives the expected acceleration due to the nonuniformity in the equations for γv_z and γv_\perp , and the drift due to the gradient of the external field in the equations for \bar{x} and \bar{y} . The latter equations do not include the curvature drift but contain additional terms, due to the fact that the axis z is defined to be the axis of the cavity and not the exact direction of the external field.

Similarly, the slow-time-scale equations for the growth rate and frequency shift of each eigenmode are:

$$\Gamma_{nm\ell} = -\frac{1}{2} \frac{\omega_{nm\ell}}{Q_{nm\ell}} + \frac{4}{1 + \delta_{nm,0}} \frac{\omega_p^2}{\omega_{nm\ell} \Omega_{nm\ell}}$$

$$\times \left\langle J_1' v_\perp \sum_{\pm} (\pm 1) (k_m \bar{c}_n \bar{s}_m \sin \zeta_{\pm} + k_n \bar{s}_n \bar{c}_m \cos \zeta_{\pm}) \right\rangle ,$$

$$\Delta_{nm\ell} = -\frac{4}{1 + \delta_{nm,0}} \frac{\omega_p^2}{\omega_{nm\ell} \Omega_{nm\ell}} \tag{12}$$

$$\times \left\langle J_1' v_\perp \sum_{\pm} (\pm 1) (k_m \bar{c}_n \bar{s}_m \cos \zeta_{\pm} - k_n \bar{s}_n \bar{c}_m \sin \zeta_{\pm}) \right\rangle ,$$

where $\delta_{nm,0} = 1$, if either $n = 0$ or $m = 0$, and $\delta_{nm,0} = 0$, otherwise, and the angular brackets denote an average over all particles inside the cavity, their number, i_{\max} , being accounted for by the beam plasma frequency, ω_p .

Let us review briefly the steps involved in the derivation of Eq. (12). The wave equation was applied on the cavity fields, expressed by the summations in Eq. (3). The orthogonality of the eigenmodes was used to decouple the wave equation, by integrating over the cavity volume after multiplying by the

appropriate trigonometric functions, with the term $1 + \delta_{nm,0}$ arising out of the different normalization when either $n = 0$ or $m = 0$. The boundary condition corresponding to the power radiated outside the cavity is accounted for by the quality factor, $Q_{nm\ell}$, which depends on the cavity and the structure (but not the amplitude) of each eigenmode. The terms $\Gamma/Q + (\Gamma^2 + d\Gamma/dt)/\omega$ and $d\Delta/dt$ are neglected compared to Δ and to $\omega/Q + 2\Gamma$, respectively, and a multiplication by $\cos\phi$ and $\sin\phi$ with omission of the fast terms leads to Eq. (12).

5. ANALYTICAL APPLICATION IN A WAVEGUIDE

Before using Eqs. (10) and (12) for any extensive study either to predict the behavior of a given oscillator or to investigate the physical processes involved in multi-mode interactions, it is prudent to first establish reliability in their correctness. This purpose is served by the present section, in which our equations are used to describe analytically a variety of situations, in order to compare these results with the appropriate earlier ones. The only configuration in our rectangular geometry, for which sufficient information exists to compare to our results, is that of an amplifier operating at a single mode. The conversion of our equations to that configuration is straightforward: it suffices to eliminate ζ_- , the backward wave dependence, to remove the meaningless term $\omega/2Q$ in the equation for Γ and to divide the equations for Γ and Δ by 2, since their derivation for the amplifier case involves an integration only over the cross section of the waveguide, and k_z has now an arbitrary value, not quantized by the meaningless z_{\max} .

First it is noted that the equations for the electrons, Eq. (10), for the special case of no nonuniformity reproduce earlier results (3), when $m=0$, $n \neq 0$, and, with an appropriate rotation of the coordinate axes, when $n=0$, $m \neq 0$. On the other hand, as noted in the previous section, the effects associated with the nonuniform external field, that is, the acceleration due to a longitudinal gradient, the drift due to a transverse gradient and the drift due to an imperfect alignment of the external field with the cavity (or waveguide) axis, are properly accounted for by our equations.

In order to see whether Eq. (12) describes the correct evolution of the fields, and because of the usefulness of a dispersion relation for arbitrary m and n , it is advisable to derive such a general relation and to compare it

to the earlier result (2) for $m=0$. In order to obtain the dispersion relation, it is assumed that Γ and Δ are constant. The equations of motion are solved self-consistently with the exponentially amplified field and, as appropriate for the high gain regime ($\Gamma t \gg 1$), the small terms are dropped. A final integration over the initial phase angle of the electrons, assumed uniformly distributed, gives the expressions for Γ and Δ , which are combined to yield the dispersion relation,

$$\alpha^2 - (k_{nm\ell}c)^2 = - \frac{2}{1 + \delta_{nm,0}} \omega_p^2 \int_0^{x_{\max}} \frac{dx}{x_{\max}} \int_0^{y_{\max}} \frac{dy}{y_{\max}} \int_0^\infty 2\pi p_\perp dp_\perp \int_{-\infty}^\infty dp_z$$

$$\times \frac{1}{Y} \left(\frac{K}{k_{nm}} \right)^2 J_1^2 R \left[(k_{nm}^\rho)^2 J_1^2 R + \left(k_{nm}^\rho - \frac{1}{k_{nm}^\rho} \right) J_1 \right] f_0 , \quad (13)$$

where $f_0(\bar{x}, \bar{y}, p_z, p_\perp)$ is the unperturbed distribution function and

$$\alpha = \omega + i\Gamma = k_{nm\ell}c + \Delta + i\Gamma ,$$

$$R = \frac{\Omega_z/\gamma}{(\alpha - \Omega_z/\gamma - k_\ell v_z)} , \quad (14)$$

$$K^2 = (k_m \bar{C}_n \bar{S}_m)^2 + (k_n \bar{S}_n \bar{C}_m)^2 .$$

Introducing into Eq. (13) a monoenergetic pencil beam, $f_0 = (x_{\max} y_{\max}) / (2\pi p_\perp) \delta(\bar{x} - \bar{x}_{\max}/2) \delta(\bar{y} - \bar{y}_{\max}/2) \delta(p_\perp - p_{\perp 0}) \delta(p_\parallel - p_{\parallel 0})$ reproduces earlier expressions. Furthermore, omitting the less important second term in brackets in Eq. (13) and confining our attention to the behavior of the dispersion relation away from the isolated (and uninteresting) real root $\alpha \approx -k_{nm\ell}c$, gives the simplified cubic relation

$$(\alpha - k_{nm\ell}c) (\alpha - k_{nm\ell}c - \theta_{+0})^2 = -\sigma_0^3, \quad (15)$$

where $\theta_{+0} = \Omega_z/\gamma_0 - k_{nm\ell} + k_\ell v_z$ is the frequency mismatch and the coupling parameter, σ_0 , is given by

$$\sigma_0^3 = \frac{1}{1 + \delta_{nm,0}} \frac{(J_1' k_{p0} \Omega_z \omega_p)^2}{\gamma_0^3 k_{nm\ell} c}. \quad (16)$$

As indicated by Eq. (15), for parameters sufficiently above threshold and for adequate synchronism, the evolution of the instability depends on the parameters θ_{+0} and σ_0^3 .

An important approximation in the derivation of Eq. (13), the dispersion relation, has been that the small argument expansion, $J_1(\Lambda) = \Lambda/2$, has been employed, where

$$\Lambda = \frac{\omega_b^2}{\Gamma^2 + (\omega - \frac{\Omega_z}{\gamma_0} - k_\ell v_{z0})^2}, \quad (17)$$

and

$$\omega_b^2 = \frac{1}{2} J_1' \frac{Kv_{z0} \Omega_{nm\ell}}{\gamma_0}. \quad (18)$$

This approximation is appropriate for the linear regime before saturation is reached, i.e., when $\Omega_{nm\ell}$ (and ω_b^2) is small. Since this approximation becomes increasingly inaccurate after $\Lambda = 1.84$ (where $dJ_1/d\Lambda = 0$) and definitely fails when $\Lambda = 3.83$ (where $J_1 = 0$), these two values give the range of Λ in which saturation is expected, $1.84 < \Lambda < 3.83$, and therefore also an estimate for the saturation amplitude, $\Omega_{nm\ell}$, from Eqs. (17) and (18).

A final application of our equations is for the case of a saturated monochromatic wave, with almost constant amplitude and frequency. Assuming that v_{\perp} and γ vary only weakly (low efficiency), then the most important variation is that of the phase angle ζ_+ , which is found to satisfy the pendulum equation,

$$\frac{d^2 \zeta_+}{dt^2} = \omega_b^2 \sin(\zeta_+ + \eta) , \quad (19)$$

where the bounce frequency, ω_b , has been defined in Eq. (18), and the reference angle η is defined by the field structure,

$$\tan \eta = \frac{k_n \bar{S}_n \bar{C}_m}{k_m \bar{C}_n \bar{S}_m} . \quad (20)$$

Both ω_b and η simplify to the known expressions (3) when $m=0$, $n \neq 0$. Furthermore, the corresponding equations for the growth rate and frequency shift of the wave give

$$\left. \begin{array}{l} \Gamma \\ \Delta \end{array} \right\} = \frac{2}{1 + \delta_{nm,0}} J_1' \frac{kv_{\perp 0} \omega_p^2}{\gamma_0 \omega_{nm\ell} \Omega_{nm\ell}} \left\{ \begin{array}{l} \langle \sin(\zeta_+ + \eta) \rangle \\ \langle -\cos(\zeta_+ + \eta) \rangle \end{array} \right\} . \quad (21)$$

In view of the electron bunching that has occurred during the exponential stage of the evolution, the evolution of the center of mass of the bunch during the nonlinear stage according to the pendulum equation, Eq. (19), schematically represented in Fig. 3, gives from Eq. (21) the characteristic one- and two-hop variation of Γ and Δ during one bounce period, shown in Fig. 4.

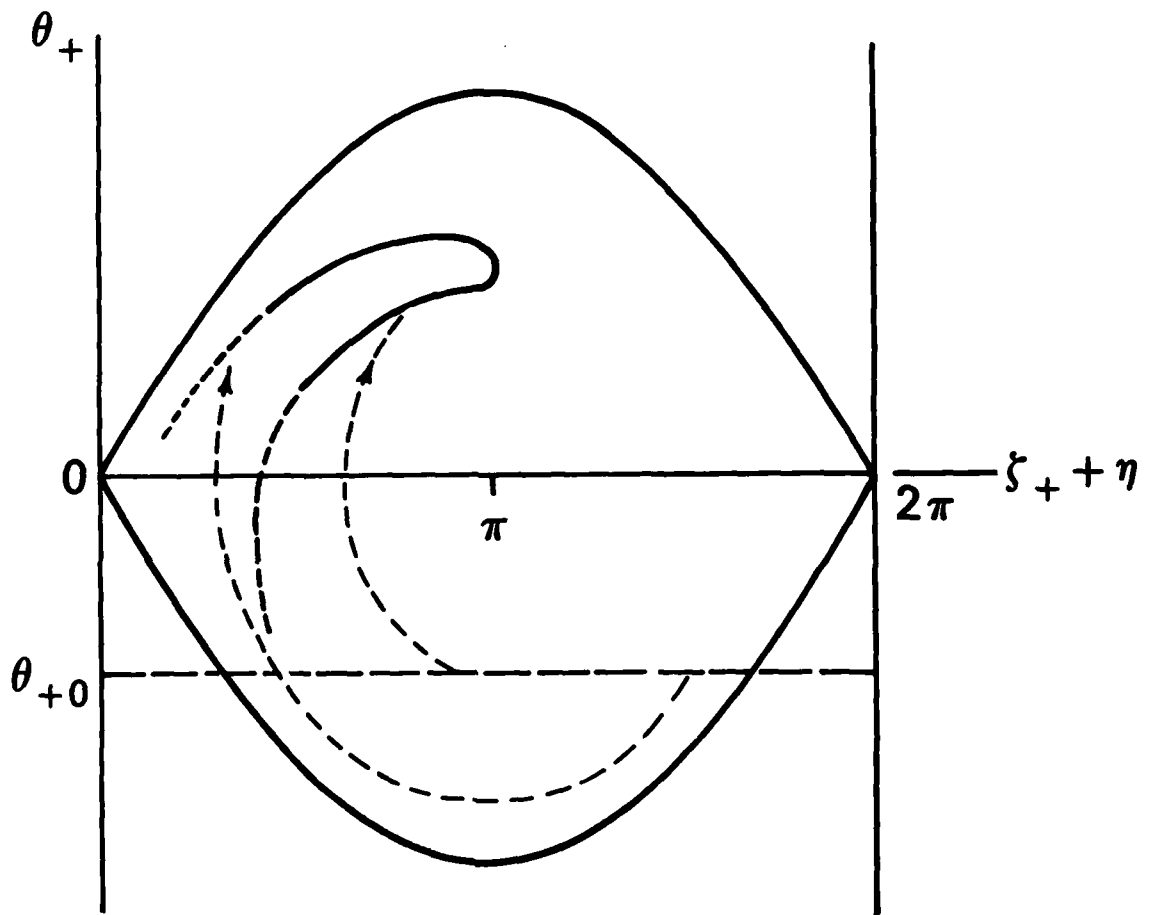


Fig. 3 - Schematic representation of the motion of the bunch.

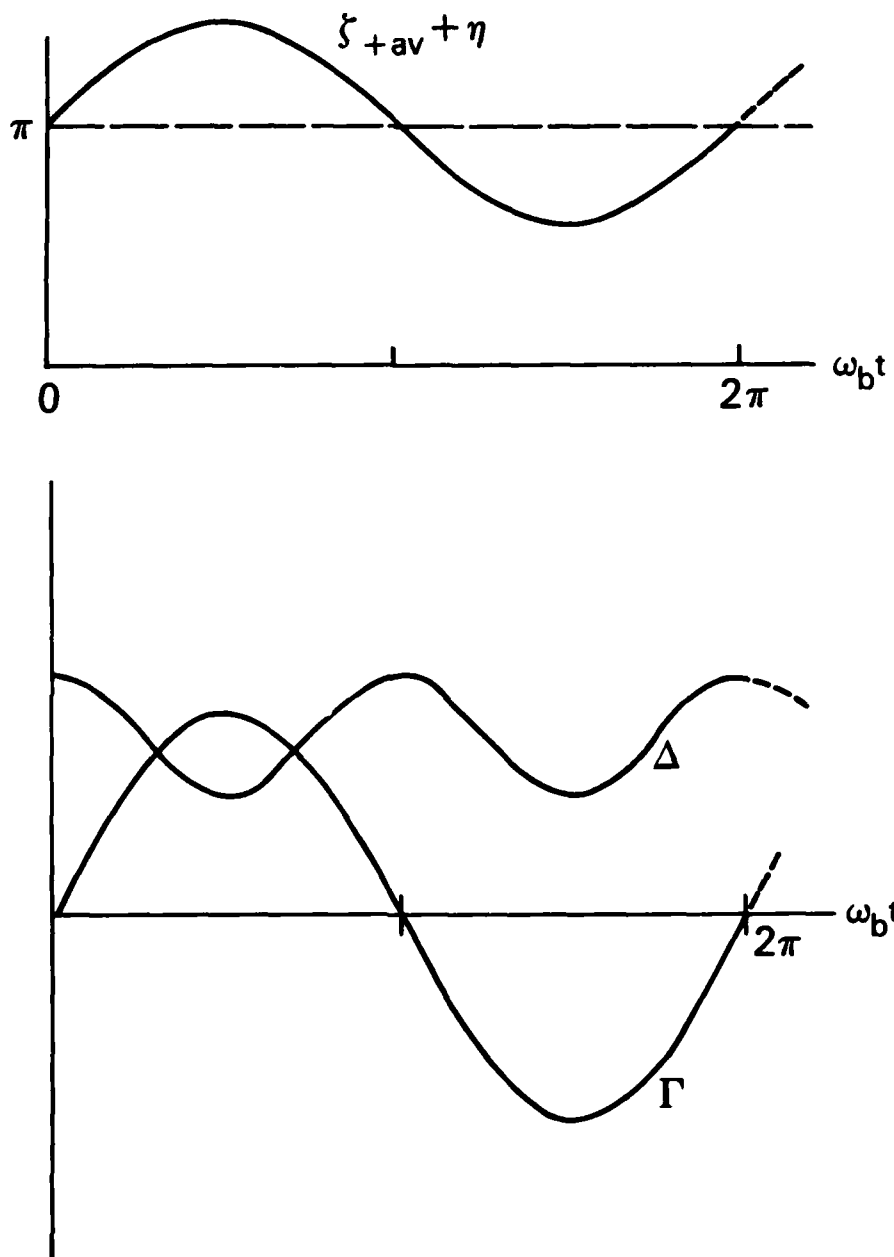


Fig. 4 - Evolution of the average relative phase of the bunch and associated evolution of the growth rate and frequency shift during a bounce period.

6. NUMERICAL APPLICATION IN A WAVEGUIDE

In the previous section we have derived equations governing various aspects of monochromatic wave evolution in a waveguide. We have shown there that these equations reproduce earlier results in the appropriate limit $m=0$, $n \neq 0$, thus establishing by implication the correctness of Eqs. (10) and (12). The next subject, covered by this section, is to establish that the algorithm based on these equations gives acceptably accurate numerical results. In all simulations discussed in this section a low amplitude monochromatic wave was initialized in a system with periodicity length $z_{\max} = 2\pi/k_{\ell}l$. The initial distribution of the electron position in z and the phase angle ψ was uniform, with the initial values assigned to each electron by the use of a random number generator, to add an experimental flavor to the results, while \bar{x} , \bar{y} , v_{\perp} and v_z were initially the same for all particles. The subsequent evolution of the electron and wave properties was obtained by a successive application of the long time-scale algorithm of Eqs. (10) and (12).

The time evolution of the amplitude, growth rate and frequency shift is shown in Fig. 5, for a simulation with $k_n = 0.958 \Omega_z/c$ ($n = 1$, $x_{\max} = 3.28 c/\Omega_z$), $k_m = 0$, $k_{\ell} = 0.108 \Omega_z/c$ ($z_{\max} = 58.0 c/\Omega_z$), $\omega_p = 10^{-3} \Omega_z$, $v_{z0} = 0.22 c$, $v_{\perp 0} = 0.26 c$, $\gamma_0 = 1.0636$ and $\bar{x}_0 = 0.5 x_{\max}$. For these values, the theoretical predictions are $\Gamma = 1.68 \times 10^{-3} \Omega_z$, $\Delta = 0.97 \times 10^{-3} \Omega_z$, to which the wave evolution is in good agreement in the linear regime. The estimate $\Lambda_{\max} = 1.84$ gives $\Omega_{\max} = 1.16 \times 10^{-4}$, comparable to the measured value $\Omega_{\max} = 1.30 \times 10^{-4}$. Finally, at saturation, oscillations are observed at the bounce frequency $\omega_b = 2.72 \times 10^{-3} \Omega_z$, as expected from Eq. (21). Some skewness in the variation of Γ and the inequality of the peaks of Δ in Fig. 5b, are accounted for by the dependence of Eq. (21) on the inverse of the wave amplitude, which was assumed to be constant when Fig. 4 was prepared.

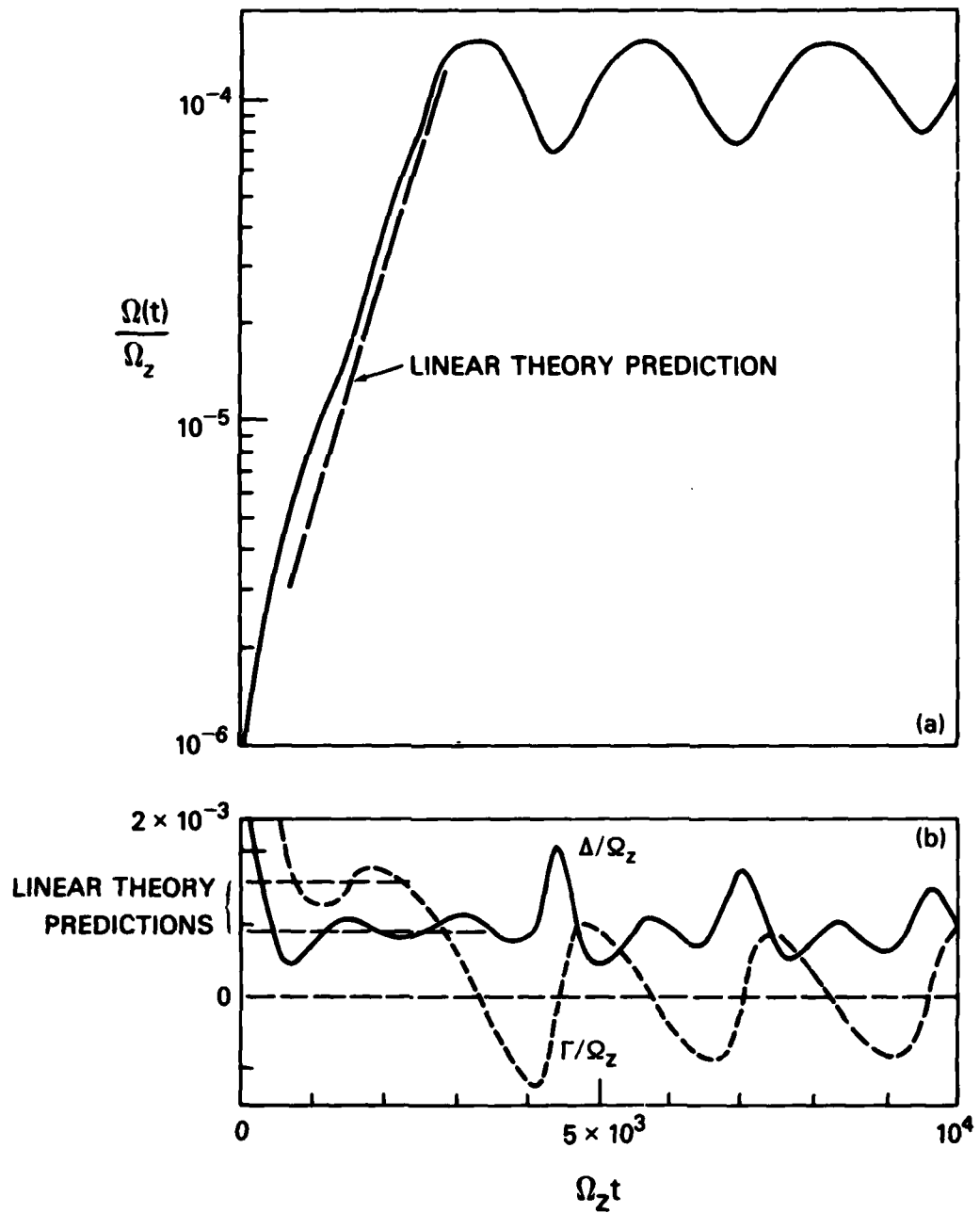


Fig. 5 - Evolution of (a) the amplitude and (b) the growth rate and the frequency shift for the reference simulation.

Some additional simulations are presented in Table 1. Case 0 is the simulation already described, which we regard as the reference simulation. The simulations of Table 1 have the same initial values as the reference case, except as indicated in the input column and discussed below. As it is seen, cases 1-5 have the appropriate scaling with regard to ω_p and v_{\perp} . The absence of amplification in case 5 is consistent with the value of v_{\perp} being below threshold. In cases 6 and 7, where the distribution of the guiding center is taken as $f(\bar{x}) = 1/\pi$ and $(\sin\bar{x})/2$ respectively, rather than $x_{\max} \delta(\bar{x} - x_{\max}/2)$, the growth rates and frequency shifts are reduced, since the average electron is acted upon by a weaker field. No amplification occurs when a delta distribution is introduced at the node of the $n=2$ field (case 8), while case 9 gives essentially the same results as case 6, consistent with the fact that the average field is independent of the number of nodes for a uniform particle distribution in \bar{x} .

The last set of numerical results are summarized in Fig. 6. In these simulations the purpose was to check the extent to which the dependence of Γ and Δ and ω_b (at saturation) satisfy the dispersion relation of Eq. (15) and the estimate $\Lambda = 1.83$, for various values of the frequency mismatch, θ_+ . The data in Fig. 6 were obtained with input parameters equal to those of the reference simulation, except for the values of Ω_2 or the periodicity length, in order to produce a variety of values for θ_+ . The quantities in Fig. 6 are scaled to the relevant parameter, σ_0 , defined in Eq. (16). As can be seen, given the difficulty of measuring these values from curves like those of Fig. 6, the agreement is very good with regard to Γ and Δ , and the saturation amplitude only slightly exceeds the value given by the estimate $\Lambda = 1.83$.

Table 1
 DEPENDENCE OF Γ , Δ and Ω_{\max} ON THE INPUT PARAMETERS
 FOR APPLICATIONS IN A WAVEGUIDE

Case	Input	r/Ω_z	Δ/Ω_z	Ω_{\max}/Ω_z
0	Reference	1.7×10^{-3}	1.0×10^{-3}	1.3×10^{-4}
1	$\omega_p/\Omega_z = 10^{-4}$	4.0×10^{-4}	2.4×10^{-4}	6.7×10^{-6}
2	$\omega_p/\Omega_z = 10^{-2}$	7.7×10^{-3}	4.5×10^{-3}	3.2×10^{-3}
3	$v_{\perp}/c = 0.6$	2.1×10^{-3}	1.4×10^{-3}	2.3×10^{-4}
4	$v_{\perp}/c = 0.1$	8.2×10^{-4}	5.0×10^{-4}	1.0×10^{-4}
5	$v_{\perp}/c = 0.01$	0	0	undef.
6	uniform distr.	1.2×10^{-3}	5.7×10^{-4}	1.3×10^{-4}
7	sine distr.	1.6×10^{-3}	6.2×10^{-4}	1.4×10^{-4}
8	$n = 2$, delta distr.	0	0	undef.
9	$n = 2$, uniform distr.	1.2×10^{-3}	5.3×10^{-4}	1.2×10^{-4}

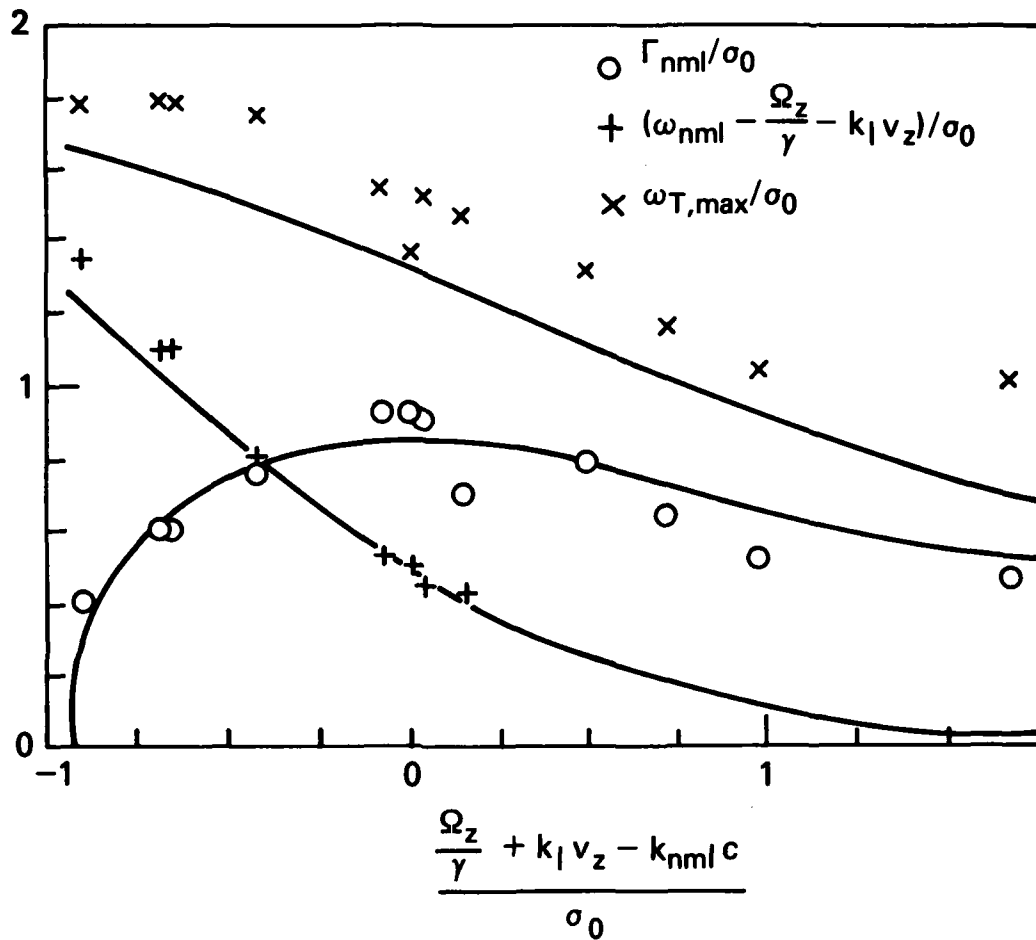


Fig. 6 - Dependence of growth rate, frequency shift and bounce frequency at saturation on the sharpness of synchronism: Comparison of the simulations to theory.

7. EFFECTS OF AN EXTERNAL FIELD NONUNIFORMITY

It has been shown theoretically that the efficiency enhancement is achieved if the external field has some nonuniformities, either in the form of a step(15) or of a constant gradient (16). The same effect has been also shown experimentally (17). A qualitative explanation of this phenomenon is that the introduction of the nonuniformity keeps the frequency mismatch, θ_+ , at favorable values over a prolonged interval, thus delaying the occurrence of saturation. Some theoretical considerations of the effects associated with the nonuniformity are given in this section. Although these considerations are of introductory nature, they may prove useful for the elucidation of the interaction.

In order to simplify the analysis, we consider the simple case in which the transverse velocity is not too much perturbed during the interaction, e.g., during the transit time in the cavity. This assumption, already employed in Sec. 5 for the derivation of Eq. (19), is rigorously applicable only when the efficiency of conversion is low, however, it is felt that the results may be extrapolatable to the high efficiency regime, at least qualitatively. In the sense of this approximation, the equation for ζ_+ is now given by

$$\frac{d^2 \zeta_+}{dt^2} = \omega_b^2 [R + \sin(\zeta_+ + \eta)] \quad , \quad (22)$$

where ω_b is defined in Eq. (18) and the effects of the nonuniformity are described by the nonuniformity ratio, R , expressing the gradient of the external field in relation to the wave field and defined by

$$R\omega_b^2 = \frac{1}{\Omega_z} \frac{d\Omega_z}{dz} \left[\omega v_z + k_\ell (v_z^2 - \frac{1}{2} v_\perp^2) \right] \quad . \quad (23)$$

Generally, the difference of the last two terms in the above definition is small compared to the first term, so that approximately $R\omega_b^2 \approx \delta(\Omega_z/\gamma)/\delta t$, where δt is the interaction duration and $\delta(\Omega_z/\gamma)$ is the corresponding change in the electron gyrofrequency.

Equation 22 represents the pendulum equation, with an added external torque expressed by R . Several features associated with this equation are presented in Ref. 22. Here it suffices to note that the condition for existence of trapped particles is

$$|R| < 1 \quad , \quad (24)$$

and that the separatrix extends approximately to the values

$$|\theta_+| \approx 2 \omega_b (1 - |R|) \quad . \quad (25)$$

For the representative case $R \approx 0.4$, the trajectories of the particles are shown in Fig. 7b, in phase space coordinates $\zeta_+ + \eta$ and $\epsilon_+ = d\zeta_+/dt$. These trajectories are to be compared to the case of a uniform external field, Fig. 7a, where by definition $R = 0$. In both cases, trapped particles like 1 and 1' execute oscillatory orbits about the vortex, which is located at $\zeta_+ + \eta = \pi$, when $R = 0$, and at $\zeta_+ + \eta = \pi + \arcsin R$, when $R \neq 0$. On the other hand, untrapped particles like 2 and 2' execute a wavy motion, when $R = 0$, never crossing the resonance line $\theta_+ = 0$, while the introduction of a nonzero value for R introduces an additional upward drift, causing untrapped particles to eventually cross the resonance line.

Based on the above remarks, but before describing the mechanism responsible for the improved efficiency when $R \neq 0$, it is convenient to discuss first the

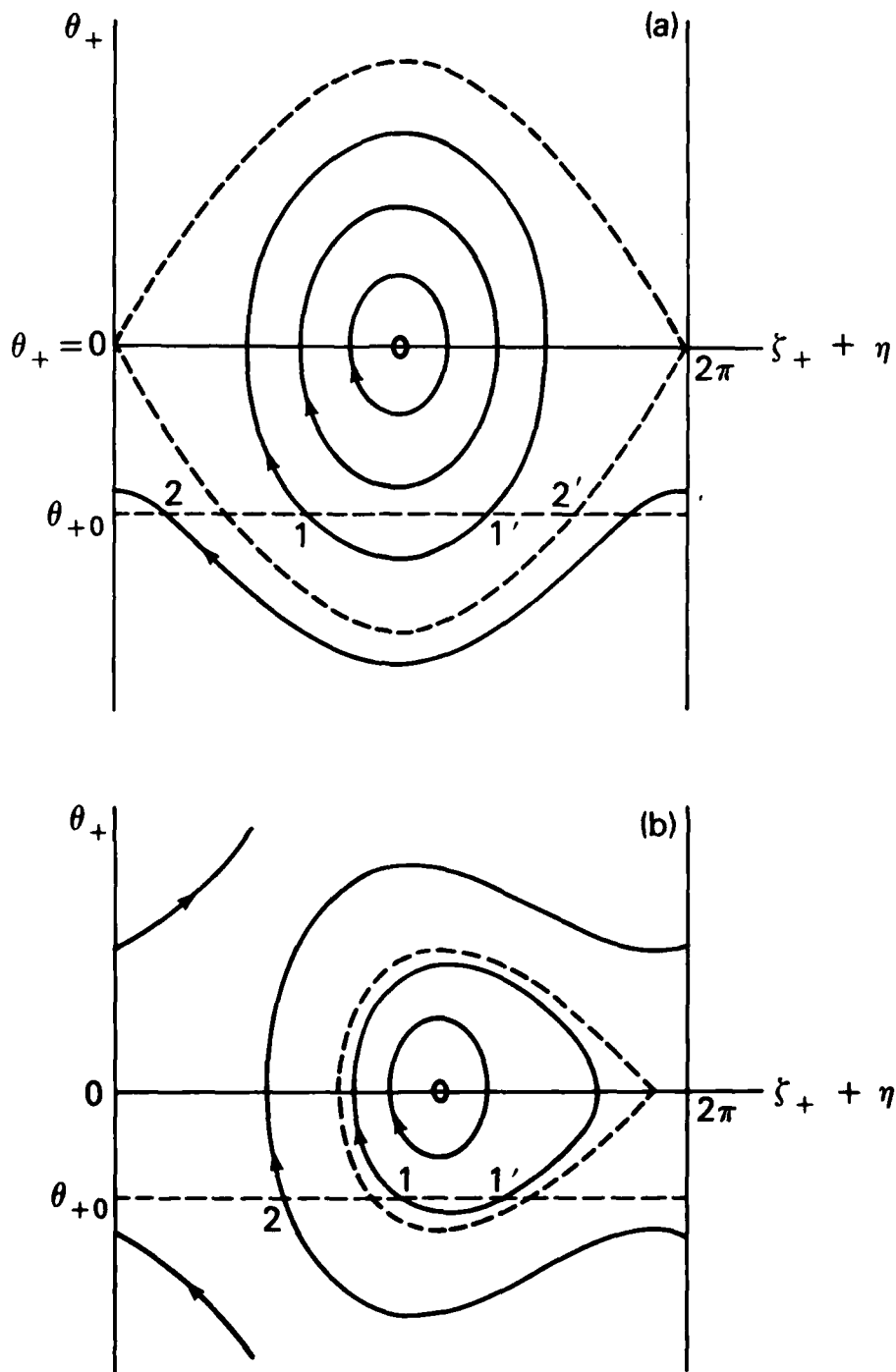


Fig. 7 - Comparison of the trajectories of particles in close resonance with a wave in (a) a uniform medium, to (b) a nonuniform medium, $R \neq 0$. The horizontal line denotes the initial conditions of the beam.

uniform case, $R = 0$, within the framework of our equations. Recalling from Eq. (21) that energy transfer from the particles to the wave is associated with $\langle \sin(\zeta_+ + \eta) \rangle > 0$, that is, when the average phase is in the interval $0 < \zeta_+ + \eta < \pi$, we note from the direction of the trapped particle motion in Fig. 7a that this interval is satisfied for interaction times, τ , such that $\omega_b \tau \lesssim \pi$, provided that $\theta_{+0} < 0$. This is also consistent with the fact that during such a time interval, the value of $\theta_+ = \Omega_z/\gamma - \omega + k_{\parallel} v_z$ increases for these particles, resulting in a decrease of γ and energy loss. The untrapped however, do not contribute to the average of $\sin(\zeta_+ + \eta)$ substantially, as can also be seen from the fact that their value of θ_t suffers weaker changes compared to the trapped particles. Accordingly, the optimal situation is determined by a trade-off between the desire for a large value for $-\theta_{+0}$, so that the average of $\sin(\zeta_+ + \eta)$ is large for the trapped particles, and for a small value for $-\theta_{+0}$, in order to reduce the percentage of idle untrapped particles.

Let us now turn our attention to the additional effects caused by the nonuniformity. We consider first the case $R > 0$ (but $R < 1$), that is of an external field increasing in the direction of the motion. This case is characterized by the transition of the untrapped particles through the line $\theta_+ = 0$ preferentially at values satisfying $\sin(\zeta_+ + \eta) > 0$, while the trapped particles oscillate about the vortex, where $\sin(\zeta_+ + \eta) < 0$. Accordingly, the desirable initial properties of the beam are those that correspond to untrapped particles. On the other hand, distant untrapped particles are not particularly attractive, since such particles will first execute a number of oscillations in $\zeta_+ + \eta = (0, 2\pi)$, before crossing the resonance line, $\theta_+ = 0$, with $\sin(\zeta_+ + \eta) > 0$. Therefore, the most effective initial arrangement for the beam is that for which $\theta_{+0} \approx -2\omega_b(1-R)$, i.e.,

the beam is initially close to the edge of the trapping region. Following the trajectories of the particles for such an initial arrangement, e.g., according to Eq. (22) or Fig. 7b, one can see that a bunch is formed, which remains over extended times in the region $\sin(\zeta_+ + \eta) > 0$. The effect of this bunch can be optimized by adjusting the value of R and θ_{+0} . However, it can be seen that the corresponding optimized efficiency will be larger when $R \neq 0$ than when $R = 0$, since the bunch is formed out of all particles, and not only out of that fraction, which is initially trapped, as is the case when $R = 0$.

The opposite situation, that of an external field gradient opposite to the direction of motion ($R < 0$, but $R > -1$), is characterized by a location of the vortex such that $\sin(\zeta_+ + \eta) > 0$. Therefore, in this case it is advantageous to arrange for a bunch to be formed out of the trapped particles, as shown in Fig. 8b. Comparing this evolution to the uniform case, it can be seen that this bunch is expected to be weaker than that of the uniform case, since the trapping region is smaller and relatively more particles will be untrapped and therefore idle, as far as the energy conversion is concerned. On the other hand, this bunch, although weaker, will be located closer to the convenient phase angle, $\zeta_+ + \eta \approx \pi + \arcsin R$, when $R < 0$. If this shift of the vortex (and bunch) phase is stronger than the reduction of the bunch density, then the efficiency for $R < 0$ will be larger than the uniform case. However, this question cannot be answered within the present qualitative discussion. It is clear, nevertheless, that if the trapped particles are allowed to execute a number of bounce oscillations, then they will contribute energy to the wave during each oscillation, since for the vortex $\sin(\zeta_+ + \eta) = -R > 0$, hence an improved efficiency is expected when $\omega_b \tau \gg \pi$, i.e., for systems with high field amplitudes (e.g., driven by high currents), or long transit times, τ , e.g., an amplifier.

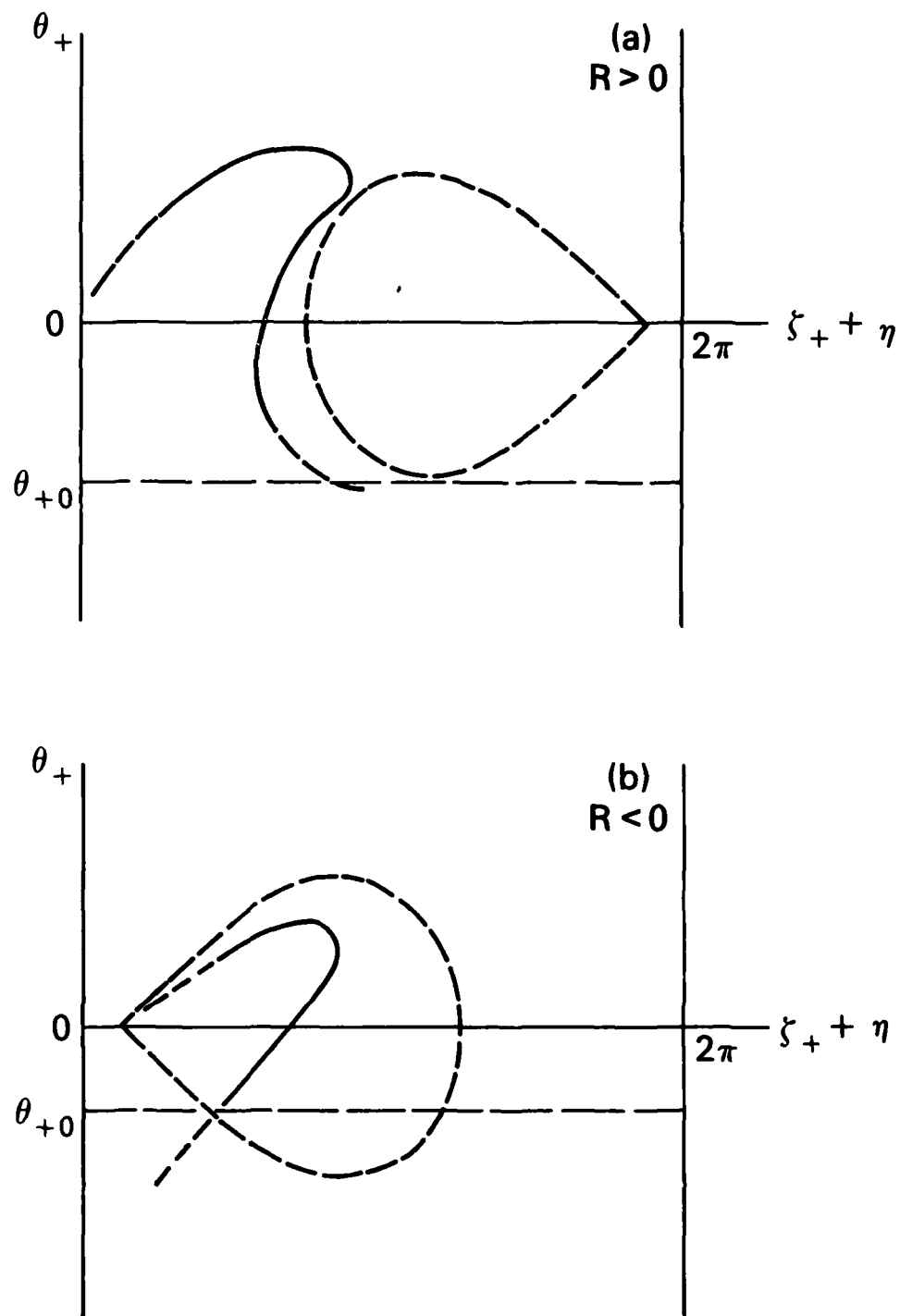


Fig. 8 - Schematic representation for the evolution of the bunch for a non-uniform external field, (a) when $R > 0$, $-\theta_{+0} \geq 2\omega_b (1-R)$, and (b) when $R < 0$, $-\theta_{+0} \leq 2\omega_b (1+R)$.

It is interesting to note that when $R \neq 0$, limitations associated with beam quality are not so severe as when $R = 0$. In the uniform case, a beam temperature associated with a spread of θ_+ , such that $\delta\theta_+ \geq \omega_b$, essentially kills the instability, since in this case the effect of a particle with initial values $\theta_{+0}, \zeta_{+0} + \eta$ is compensated by that of a particle at $-\theta_{+0}, 2\pi - (\zeta_{+0} + \eta)$. This is not the case, however, when a nonuniformity is introduced. For example, when $R > 0$, the external field can be adjusted so that at the entrance of the cavity $\theta_+ < -2\omega_b(1 - R)$ for all particles. The ensuing motion of these untrapped particles (Fig. 9a) will bring them near resonance, where they will occupy a region with $\langle \sin(\zeta_+ + \eta) \rangle > 0$, transferring energy to the wave. Similarly, when $R < 0$, the initial value of θ_+ can be arranged to be on the average close to zero. Then, the untrapped particles will eventually leave the resonance region, spread uniformly in ζ_+ , while the trapped particles will remain inside the separatrix, with $\langle \sin(\zeta_+ + \eta) \rangle > 0$. The case $R > 0$ is particularly adoptable to a cavity, since energy conversion is limited to the time it takes the untrapped particles to move around the separatrix, while the case $R < 0$ is primarily applicable to an amplifier, to take advantage of the extended time, over which the trapped particles are able to convey energy to the wave. In either case, calculations for the corresponding efficiencies can be made based on the data of Ref. 22.

Finally, it can be seen that mathematically the introduction of a gradient in the external field is equivalent to a variation of the cavity cross section, since both cause θ_+ to vary independently of the cavity fields. A generalized expression can be written for R ,

$$R\omega_b^2 = \frac{d}{dt} \theta_+ = \frac{d}{dt} \left(\frac{\Omega_z}{\gamma} - \omega + k_x v_z \right), \quad (26)$$

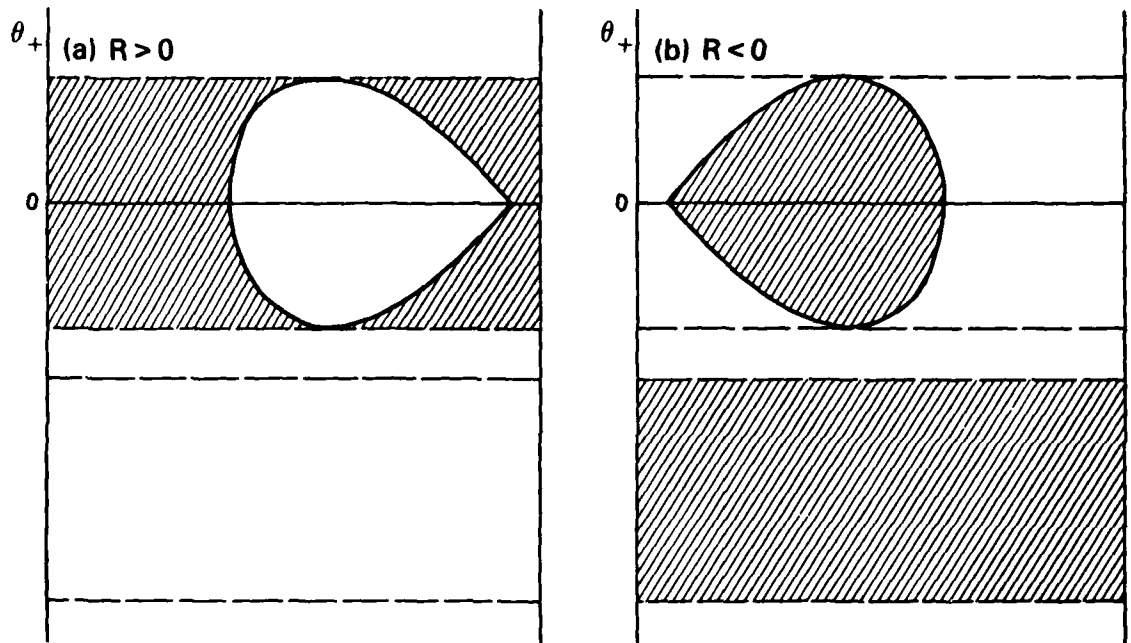


Fig. 9 - Schematic representation for the evolution of a beam with temperature, (a) when $R > 0$, with no particles initially trapped, and (b) when $R < 0$, with the trapping region initially filled.

with the derivative being evaluated in the absence of the cavity fields. When $d\Omega_z/dz \neq 0$, Eq. (26) yields the expression already presented (Eq. (23)). A variable cross section causes k_ρ to be a function of z , since $k_\rho^2 = (\omega/c)^2 - \pi^2(n^2/x_{\max}^2(z) + m^2/y_{\max}^2(z))$, hence the corresponding expression for R is

$$R\omega_b^2 = v_z^2 \frac{dk_\rho}{dz} \quad (27)$$

In addition, an alternate situation where Eq. (27) is applicable is when the cavity is lined with a thin and weak dielectric material, with its dielectric constant varying with z , while an appropriate expression can be obtained from Eq. (26) when a weak electrostatic field is externally applied along the axis of the cavity.

8. APPLICATION TO AN OVERMODED CAVITY

In this section we present and discuss various results obtained from the numerical application of the algorithm formed from Eqs. (10) and (12) to the case of a rectangular cavity, in which more than one eigenmode is in close resonance with the beam. We have chosen the parameters so that they correspond as closely as possible to those of typical NRL experimental arrangements. Thus, the electron beam was chosen with initial velocities $v_{z0} = 0.267c$ and $v_{\perp 0} = 0.400c$, giving a relativistic factor of $\gamma_0 = 1.14$ and an anisotropy ratio $v_{\perp 0}/v_{z0} = 1.50$, typical of the NRL beam. The dimensions of the rectangular cavity were $z_{\max} = 33.10 c/\Omega_z$ in length, $x_{\max} = 6.78 c/\Omega_z$ in width, with the height, y_{\max} , sufficiently short, so that only the modes with $m = 0$ can be resonant. In this cavity, resonant modes are those with $n = 2$, hence $k_n = 0.927 \Omega_z/c$, and with $\ell = 1$ and $\ell = 2$, corresponding to $k_\ell = \ell \times 0.095 \Omega_z/c$. This choice gives a ratio of k_n/k_ℓ equal to the corresponding ratio in the NRL cylindrical cavity with a length to diameter ratio of 4, with the coordinates (x, y, z) corresponding to (r, θ, z) of the cylindrical geometry and x_{\max} corresponding to the diameter. The beam is placed at $\bar{x} = 0.33 x_{\max}$, since at that point the ratio $E_y/B_z = \tan(k_n \bar{x}) = 1.84$ is equal to the corresponding value at E_θ/B_z for the cylindrical cavity at the point where E_θ is maximum. The corresponding values of the empty cavity frequencies are $\omega_1 = 0.932 \Omega_z$ and $\omega_2 = 0.946 \Omega_z$, the frequency mismatches relative to the forward components of these modes are $\theta_{+1} = -2.95 \times 10^{-2} \Omega_z$ and $\theta_{+2} = -1.85 \times 10^{-2} \Omega_z$, where the subscripts refer to ℓ , the axial harmonic number. The transit time of the electron through the cavity is $\tau = z_{\max}/v_{z0} = 124 \Omega_z^{-1}$ and at the position of the beam the effective transverse wavenumber, defined by Eq. (14c), is $K = k_n \sin(k_n \bar{x}) = 0.811 \Omega_z/c$.

For the numerical implementation of our slow-time-scale algorithm, the cavity is initially assumed empty, with low amplitude standing cavity waves.

The beam electrons are initialized all with the same values for \bar{x} , v_z , v_\perp , as given above, while their initial position, $z_0 < 0$, and phase angle, ψ_0 , are given a uniform distribution by use of the random number generator. The electrons advance according to Eq. (10), if inside the region of interaction, $0 < z < z_{\max}$, and according to unperturbed cyclotron motion, given by Eq. (6) when outside the cavity. Depending on the density (or current) that the simulation electrons represent, it was found that approximately 100 to 300 electrons suffice to yield accurate statistics, while an accurate integration of their equation of motion is obtained with a time step, Δt , ranging from 1/8 to 1/15 of the transit time. Because of the continuous positioning of the electrons along the z-axis, they do not, in general, cross the boundaries at the quantized multiples of Δt , hence for electrons near the boundaries the algorithm is applied over the effective time of interaction, that is, the fraction of Δt which corresponds to motion inside the cavity. Finally, since electrons that cross the exit boundary do not contribute to the interaction any more, they are "destroyed" and their memory locations in the computer is occupied by properties of electrons, which are about to enter the cavity. This procedure results in substantial savings on the size of memory required, since the transit time is a very small fraction of the total time required to observe a semblance of a steady state. In implementing this procedure, care has been exercised to assure that a uniform particle density in z is maintained, before they enter the cavity.

In Table 2, we present the results of ten simulations for the cavity and modes presented above. In these simulations the quality factors are $Q_1 = 1000$ and $Q_2 = 700$, and the simulation electrons represent different plasma densities, as given by the value of ω_p . In cases 1-6 and 10, both modes are initialized

Table 2

CHARACTERISTICS OF THE EVOLUTION OF THE DOMINANT MODE
 IN A TWO-MODE CAVITY WITH $Q_1 = 1000$ and $Q_2 = 700$.
 THE MODES DENOTED BY AN ASTERISK HAVE BEEN PRIMED.

Case	ω_p/Ω_z ($\times 10^{-2}$)	Dominant mode	Γ/Ω_z ($\times 10^{-3}$)	Ω_{\max}/Ω_z ($\times 10^{-2}$)	ω_b/Ω_z ($\times 10^{-2}$)	Ω_{\max}/ω_p	$\omega_b\tau$	$-\theta_+/ \omega_b$	η (%)
1	0.8	2	0.24	0.77	2.26	0.96	2.80	0.82	14.5
2	1.0	2	0.80	0.98	2.53	0.98	3.15	0.73	14.6
3	1.2	2	1.52	1.22	2.84	1.02	3.52	0.65	16.0
4	1.5	2	2.4	1.70	3.35	1.13	4.16	0.55	19.5
5	2.0	2	3.3	2.10	3.72	1.05	4.61	0.50	17.0
6	3.0	2	6.4	2.90	4.38	0.97	5.43	0.42	14.4
7	4.0	2*	-	3.15	4.56	0.79	5.65	0.41	9.7
8	0.8	1*	-	1.36	3.00	1.70	3.72	0.98	30.1
9	2.0	1*	-	3.02	4.46	1.51	5.53	0.66	23.7
10	4.0	1	9.6	4.71	5.58	1.18	6.91	0.53	14.6

with a low amplitude, $\Omega = 10^{-3} \Omega_z$, and one mode became dominant, as denoted in the Table. This mode was initially amplified essentially exponentially, at a rate given by Γ , and later approached an oscillatory asymptotic saturation, with the value Ω_{\max} and the corresponding value for the bounce frequency, ω_b , as given in the Table. Additional entries in the Table are the ratio Ω_{\max}/ω_p , the product $\omega_b \tau$ of the bounce frequency times the transit time, the ratio $-\theta_+/\omega_b$ of the frequency mismatch to the bounce frequency, and the efficiency, η , of conversion, defined by Eq. (4) as the ratio of radiation to beam entry power. Cases 7-9 are a repetition of cases 10, 1, and 5, except that the nondominant mode of the original cases was initially primed to a value of $10^{-2} \Omega_z$ for the amplitude. This resulted in these modes becoming artificially dominant, with parameters at saturation as given in the Table.

Typically, the evolution of the amplitude and frequency of the two modes is as shown in Fig. 10, where the actual values of the parameters are those of case 4. The dominant mode, which here is that with $\ell=2$, is seen to grow exponentially, with a weak oscillation superposed, and later to approach an asymptotic state. The nondominant mode initially attempts to grow, at a weaker rate and with relatively stronger oscillations, reaching a maximum amplitude with a value depending on the beam density. The peak amplitude is always reached near the time of transition from the exponential amplification to approach to equilibrium of the dominant mode. Beyond that time, the nondominant mode decays on the average, while the oscillations persist. In all simulations the period of these oscillation is equal to $450 \Omega_z^{-1}$, equal to the beat period, $2\pi/(\omega_2 - \omega_1)$, of the two modes. Oscillations of the same period are also present in the amplitude of the dominant mode, however these oscillations are too weak to be seen in Fig. 10. With regard to the frequency plots, one first notes a relatively wide dispersion in the data points,

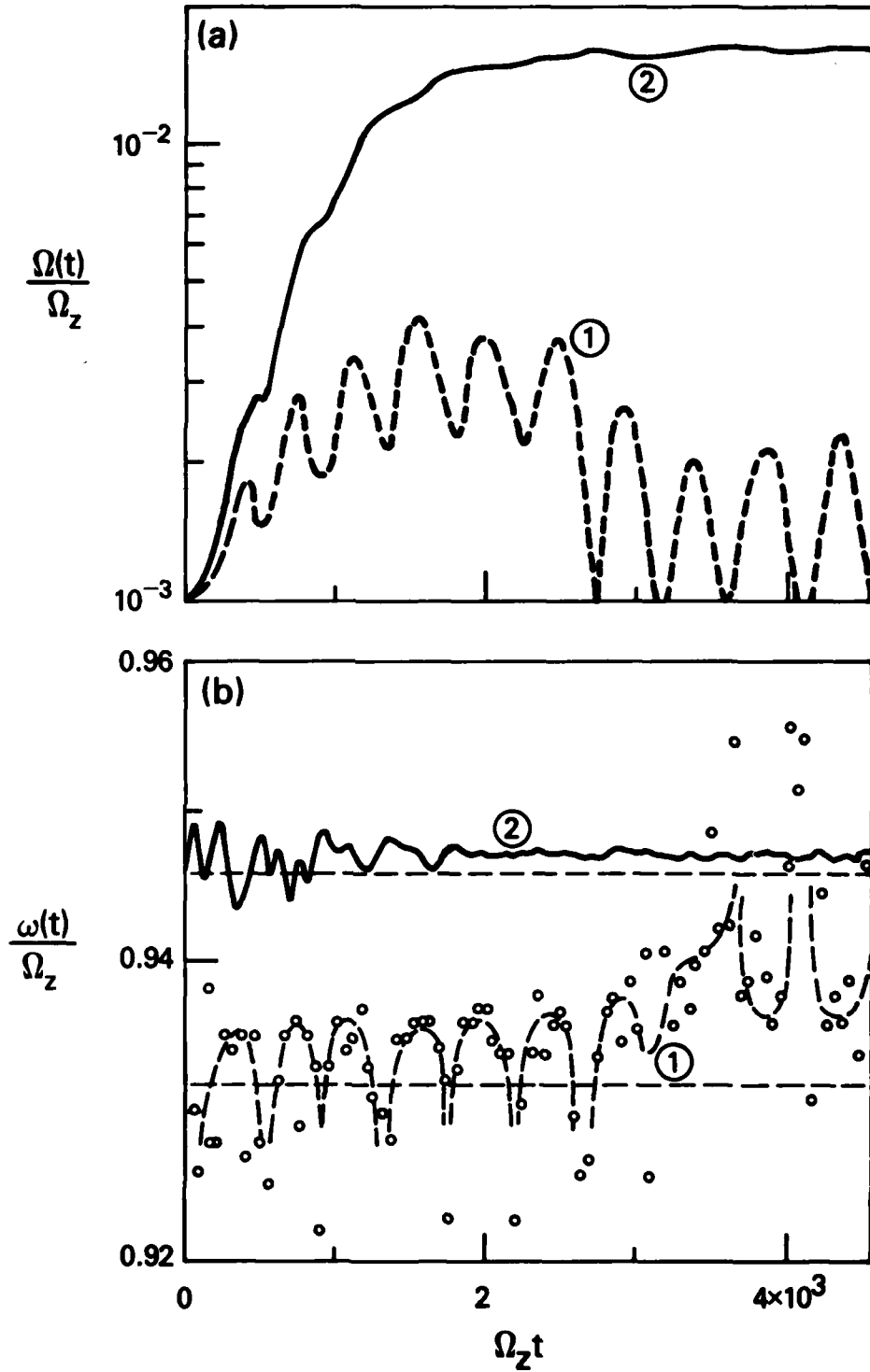


Fig. 10 - Evolution of the (a) amplitude and (b) frequency of the resonant modes for case 4 of Table 2. The horizontal broken lines in (b) give the empty cavity frequencies.

primarily during the initial evolution of the $\ell=2$ mode and always for the $\ell=1$ mode. The dispersion is directly related to the fluctuations associated with the randomness in the particle initialization. Similar fluctuations are present in the evolution of the growth rates. Such fluctuations are of no major concern, since they affect only the instantaneous values, Γ and Δ , while particle dynamics are governed primarily by the wave amplitudes and phases, which are much smoother (see Figs. 10a and 11) being integrated values. Apart from these fluctuations, it can be seen that the frequency of the dominant mode essentially approaches a constant value, shifted from the empty cavity value by approximately 1%, while the frequency of the $\ell=1$ mode has similar beat oscillations, like the amplitude.

In all cases of Table 2, and in many more two-mode cases not presented here, the asymptotic behavior of the spectrum is dominated by one mode, the amplitude and energy of the additional mode being respectively one and two orders of magnitude smaller. In such cases, it is appropriate to treat the nondominant mode as a stable perturbation driven by a constant amplitude monochromatic field, while the dynamics of the electrons is determined by the large amplitude field only. If we assume that the motion of the particles is adequately represented by the pendulum equation, Eq. (19), in the limit of small oscillations about $\zeta_+ + \eta = \pi$, then integrating $\sin(\zeta_+ + \eta)$ over the transit time, substituting this time average in place of the ensemble average in Eq. (21a), with Γ replaced by $\omega/2Q$, as is appropriate for a steady state oscillator, and using also the definition of ω_p , Eq. (18), with $J_1^2 = 0.5$, one obtains a relation for the amplitude of the dominant mode,

$$\left(\frac{\Omega_{\max}}{\omega_p}\right)^2 = f \frac{32}{1 + \delta_{nm,0}} \frac{\gamma_0 Q}{\omega \tau} \frac{-\theta_{+0}}{\omega}, \quad (28)$$

and accordingly, the efficiency is obtained from Eq. (4),

$$\eta = f \frac{2\gamma_0}{\gamma_0 - 1} \frac{-\theta_{+0}}{\omega} \left(\frac{\omega}{k_{nm}c} \right)^2 \quad (29)$$

The above equations demonstrate the known fact that the wave frequency must exceed the gyrofrequency, i.e., $\theta_{+0} < 0$, in order for positive energy conversion to be possible. The coefficient f has the value $f = 1$ in the idealized situation when the pendulum equation is applicable, the bunch is perfect and consists of all particles, and the bunch performs half of a bounce oscillation during transit. Deviations from such idealized conditions reduce somewhat the value of f . For the simulations already discussed, the idealized values of Ω_{\max}/ω_p , from Eq. (28) when $f = 1$, are 2.24 and 1.45, for the $\ell=1$ modes respectively, and as can be seen from Table 2, depending on $\omega_b\tau$ and θ_{+}/ω_b , the actual values of Ω_{\max}/ω_p indicate that $f \lesssim 0.6$. The same holds true also for the simulations not presented here.

Let us turn our attention now on the effects which the large amplitude wave has on the nondominant one. Since the bunch is attached to the dominant mode, the current it represents will alternately act constructively or destructively on the secondary mode, depending on whether they are in or out of phase. This succession is repeated at the beat period, as observed in the simulations. Similarly, due to the oscillations of the reactive component of the current relative to the low amplitude wave, its frequency oscillates about the empty cavity value. This can be seen in Fig. 10b up to the time $t = 3000$. However, beyond that time, which incidentally coincides with the time the dominant mode amplitude has practically reached the final saturation value, the frequency of the driven mode appears to oscillate about that of the dominant mode. This can be better seen in Fig. 11, where the phase of mode $\ell=1$ relative to that of $\ell=2$, $\phi_1 - \phi_2$, is plotted against time, the latter in

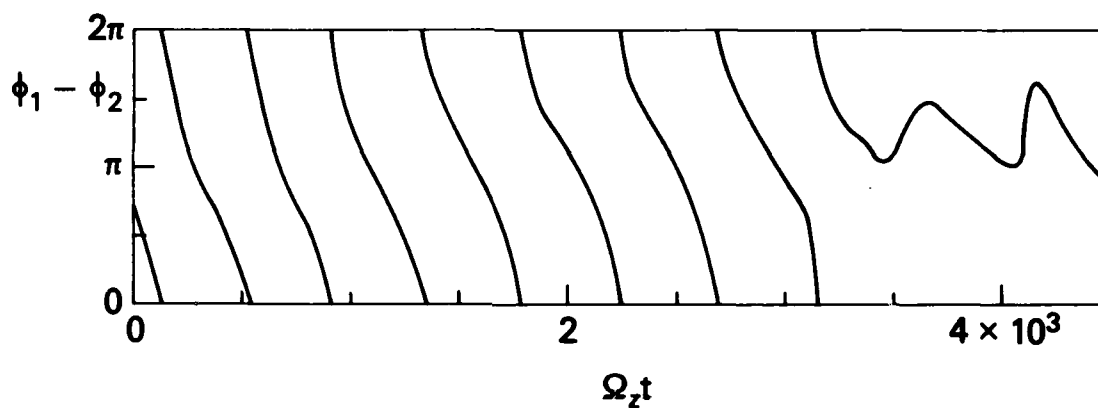


Fig. 11 - Relative phase of mode 1 to mode 2, $\phi_1 - \phi_2$, versus time for the simulation of Fig. 10.

an expanded scale compared to Fig. 10, for improved clarity. It can be seen there that the relative phase initially executes a number of complete rotations, during which it preferentially remains a relatively longer time in the vicinity of $\phi_1 - \phi_2 = \pi$, at times which coincide with the occurrence of maxima in the amplitude. However, after the initial complete rotations, the relative phase appears locked in the interval $\pi < \phi_1 - \phi_2 < 3\pi/2$, and accordingly, the frequency of the $\ell=1$ mode oscillates about that of the $\ell=2$ dominant mode.

Before concluding, let us point out that in all two-mode simulations, those of Table 2 and those not presented here, only one mode seems to dominate. This mode is not necessarily the one corresponding to the highest amplitude or efficiency. For example, the amplitude and efficiency of the dominant $\ell=2$ mode in cases 1 and 5 are significantly below the corresponding values of the $\ell=1$ mode, if the excitation of the latter is assured through priming, as is done in cases 8 and 9. The opposite holds true in a comparison of case 10 to case 7. On the other hand, simulations of a long cavity, in which many modes are resonant with the beam, ranging from $\ell=1$ to $\ell=10$, have shown that many of these modes are simultaneously excited to comparable amplitudes and efficiencies. Such situations have not been adequately analyzed at this time, and accordingly we choose not to present them here.

9. DISCUSSION

In this work we have developed the self-consistent formalism for the interaction of the eigenmodes with the electron beam in an overmoded gyrotron cavity. The resulting equations have been applied in various simplified situations, both analytically and numerically, in order to establish their correctness, to extend earlier results, to interpret the effects of an axial nonuniformity and to initiate the investigation of the multi-mode interactions. The approach we have adopted, discussed in Sec. 3, consists of an integration over the fast-time scale, which includes variations at the wave and the electron cyclotron frequencies, resulting in equations depending only on first order parameters describing the amplitude of the cavity fields and the non-uniformities, and varying only at the slow-time scale characterized by the bounce frequency and the relative frequencies. The derivation of these equations was discussed in Sec. 4. In addition to self-consistency, Eqs. (10) and (12) have the advantages of applicability to analytical investigations and of high efficiency when used in numerical simulations.

The correctness of the equations was established in Sec. 5, and the accuracy of their numerical implementation was demonstrated in Sec. 6, by applying a simplified version of the equations to study the evolution in a rectangular waveguide. Our analysis has enabled us to derive general expressions for the dispersion relation and for the bounce frequency for the case of arbitrary variations of the wave in both transverse directions. These results are represented by Eq. (13) (or Eq. (15) for conditions well above threshold) and Eq. (18). In addition, a dimensionless parameter, Λ , was obtained in Eq. (17), which is useful to determine the saturation level of the instability, and simplified equations were obtained for the particle dynamics and wave evolution at saturation (see Eqs. (19) and (21)).

The subject of external axial nonuniformities was considered in Sec. 7. The equations of motion were simplified to the pendulum equation, Eq. (22), with an external torque, given by R in Eq. (23) (or Eqs. (26) or (27)) representing the effects of the nonuniformities. Based on the corresponding electron trajectories, the efficiency enhancement was interpreted when $R > 0$, while the possibility of similar effects was discussed for the case $R < 0$, under the appropriate conditions. It was also shown that a positive efficiency should be expected also in the case of a beam with substantial thermal spread, both when $R < 0$ and $R > 0$, under conditions roughly representative of an oscillator and amplifier, respectively. Finally, the equivalence of a multitude of nonuniformities was shown. Such nonuniformities include a gradient of the external magnetic field, a gradient in the cross section, the presence of an axial static electric field and the introduction of a dielectric material with a dielectric constant which depends on position.

Some introductory investigation of two-mode competition has been presented in Sec. 8. It was seen that one mode eventually dominates the spectrum and effectively suppresses the excitation of the second mode, regardless of whether or not the unamplified mode would have reached higher power levels, were it permitted to grow alone. This behavior is similar to that observed by Dialetis and Chu (21). Analytical expressions for the saturation amplitude and efficiency were obtained, see Eqs. (28) and (29), and satisfactorily verified by the simulations. Finally, it was shown that the asymptotic behavior of the system is characterized by amplitude and frequency oscillations at the beat frequency. It can easily be seen that such oscillations correspond to a weak excitation of a discrete sideband spectrum with separation equal to the frequency difference of the two modes. It is possible that the simultaneous excitation of many modes in a highly overmoded cavity is related to the

corresponding denseness of this spectrum parts of which might well resonate effectively to different eigenmodes.

At this point it is appropriate to present a discussion on the limitations of the test particle analysis by Dialetis and Chu (21). One limitation in their approach is related to the absence of self-consistency, caused by the omission of the reactive component of the current. This suppresses any shift, Δ , of the frequency from its empty cavity value, causing incorrect conclusions to be drawn when this shift is important. Such a situation would arise when the frequency shift is comparable to, or larger than, either the frequency mismatch, or the inverse transit time, that is, either $\Delta/\theta \geq 1$ or $\tau \Delta \geq 1$, since in such cases one would obtain inaccurate evaluations of the motion of the trapped or untrapped particles, respectively. In general, however, $\Delta \sim \omega/Q$, as can be seen from Eq. (12), hence the parameters they consider satisfy $\Delta/\theta \sim \tau \Delta \sim 0.1$, and no danger of substantial error appears present. More serious could be their assumption on the existence of a steady state. As has been shown in our simulations, the equilibrium state is not steady, but oscillatory. These oscillations may be very important when more than two modes are simultaneously present, because of the possibility of synchronism between parts of the discrete spectra, which such oscillations represent.

In conclusion, let us discuss various extensions and modifications to our work. One desirable modification appears to be that associated with the adoption of a cylindrical geometry, which is more compatible with the experimental arrangements. No conceptual difficulty is expected, with the method of Sec. 3, including Eq. (6) being directly applicable. The eigenmodes will have a different transverse dependence, and the only added feature will be the application of Graf's addition theorem in the evaluation of the fields along the zero order trajectories, e.g.,

$$J_m(k_n r) \cos(m\theta) = \sum_{q=-\infty}^{+\infty} J_{m+q}(k_n \bar{r}) J_q(k_n \rho) \cos [m(\theta - \bar{\theta}) + q(\pi + \psi - \bar{\theta})], \quad (30)$$

where $\tan \bar{\theta} = \bar{y}/\bar{x}$ and $\tan \theta = y/x$, while here n and m are the radial and azimuthal harmonic numbers.

A second possible extension, independent of the choice of rectangular or cylindrical geometry, involves the introduction of alternate axial nonuniformities. The additional force due to an axial electric field is a trivial extension, while the inertial forces produced by a variation of the cross section and the introduction of a dielectric sleeve with position dependent dielectric constant can be accounted for by assigning a WKB-type axial field dependence, of the form $\sin k_z z$, where k_z is now a function of z , calculated in terms of the frequency and the local value of the transverse wave number. In addition, and regardless of the above, calculations have to be performed to extend the definition of R (Eq. (23)) to the high efficiency regime, to investigate the dependence of efficiency enhancement on R , and to assess the effects of the direction of the nonuniformity and the possibility of obtaining acceptable values for the efficiency in spite of a thermal spread, as discussed in Sec. 7.

Finally, the introductory results of Sec. 8 are expected to be useful in various aspects of the study of multi-mode competition. An interesting first step appears to be the investigation of particle trajectories in a two-mode field, with a steady large amplitude dominant mode accompanied by an oscillatory low amplitude secondary mode, to establish criteria for the stability of such a configuration. The following step would be to study the effects of coupling between harmonics of the beat frequencies in a highly overmoded cavity, in which more than two resonant modes are present. In addition, the competition of modes with different transverse structure should be considered.

Clearly, all these subjects are to be pursued primarily numerically, with supporting analytical considerations to the extent it is feasible.

ACKNOWLEDGMENTS

During various stages of this work, discussions with K. R. Chu, D. J. Dialetis, V. L. Granastein, M. E. Read and W. M. Manheimer have been very helpful.

This work was supported in part under U. S. Department of Energy Contract No. EX-77-A-34-1015.

REFERENCES

1. A. V. Gaponov, M. I. Petelin, and V. K. Yulpatov, Radiophys. Quantum Electron, 10, 794 (1967).
2. Edward Ott and Wallace M. Manheimer, IEEE Trans. PS-3, 1 (1975).
3. P. Sprangle and Wallace M. Manheimer, Phys. Fluids 18, 224 (1975).
4. V. L. Granatstein, P. Sprangle, M. Herndon and R. K. Parker, J. Applied Phys. 46, 2021 (1975).
5. V. A. Flyagin, A. V. Gaponov, M. I. Petelin, and V. K. Yulpatov, IEEE Trans. MTT-25, 514 (1977).
6. J. L. Hirshfield and V. L. Granatstein, IEEE Trans. MTT-25, 522 (1977).
7. P. Sprangle and A. T. Drobot, IEEE Trans. MTT-25, 528 (1977).
8. W. M. Manheimer and V. L. Granatstein, NRL Memorandum Report 3493 (1977).
9. A. A. Andronov, V. A. Flyagin, A. V. Gaponov, A. L. Gol'denberg, M. I. Petelin, V. G. Usov, and V. K. Yulpatov, Infrared Physics 18, 385 (1978).
10. H. Jory, S. Hegji, J. Shiverly and R. Symons, Microwave J. 21, 30 (1978).
11. K. R. Chu, Phys. Fluids 21, 2354 (1978).
12. J. Mark Baird, 1979 IEEE International Electron Devices Meeting Technical Digest, p. 156.
13. D. V. Kisel', G. S. Korablev, V. G. Navel'yev, M. I. Petelin, and Sh. Ye. Tsimring, Radio Engineering and Electronics Physics 19, 95 (1974).

14. Yu. V. Bykov and A. L. Gol'denberg, Radiophys. Quantum Electron. 18, 791 (1975).
15. P. Sprangle and Robert A. Smith, NRL Memorandum Report 3983 (1979).
16. K. R. Chu, M. E. Read, and A. K. Ganguly, NRL Memorandum Report 4051 (1979).
17. M. E. Read, K. R. Chu, and A. J. Dudas (to be published).
18. M. A. Moiseev, G. S. Nusinovich, Radiophys. Quantum Electron. 17, 1305 (1974).
19. G. S. Nusinovich, Radiophys. Quantum Electron. 19, 1301 (1976).
20. I. G. Zarnitsyna and G. S. Nusinovich, Radiophys. Quantum Electron. 20, 313 (1977).
21. D. J. Dialetis and K. R. Chu (to be published).
22. J. L. Vomvoridis and J. Denavit, Phys. Fluids 22, 367 (1979).
23. J. L. Vomvoridis and J. Denavit, Phys. Fluids 23, 174 (1980).
24. C. E. Rathmann, J. L. Vomvoridis, and J. Denavit, J. Comput. Phys. 26, 408 (1978).
25. J. L. Vomvoridis and P. Sprangle, Fourth International Conference on IR and MM Waves, Conference Digest, S. Perkowitz, Editor, pp. 101-103, (1979).

DISTRIBUTION LIST*

Naval Research Laboratory
4555 Overlook Avenue, S.W.
Washington, D.C. 20375

Attn: Code 1000 - CAPT E. E. Henifin
1001 - Dr. A. Berman
4700 - Dr. T. Coffey (25 copies)
4701 - Mr. J. Brown
4740 - Dr. V. L. Granatstein (20 copies)
4740 - Dr. K. R. Chu
4740 - Dr. C. W. Roberson
4740 - Dr. M. E. Read
4790 - Dr. P. Sprangle (100 copies)
4790 - Dr. M. Lampe
4790 - Dr. W. M. Manheimer
6603S- Dr. W. W. Zachary
6650 - Dr. L. Cohen
6656 - Dr. N. Seeman
6805 - Dr. S. Y. Ahn
6805 - Dr. A. Ganguly
6805 - Dr. N. R. Vanderplaats
6850 - Dr. L. R. Whicker
6875 - Dr. R. Wagner

On Site Contractors:

Code 4740 - Dr. J. M. Baird (B-K Dynamics)
4740 - Dr. L. Barnett (B-K Dynamics)
4740 - Dr. D. Dialetis (SAI)
4740 - Dr. Y. Y. Lau (SAI)
4740 - Dr. J. S. Silverstein (HDL)
4790 - Dr. A. T. Drobot (SAI)
4790 - Dr. C. M. Tang (JAYCOR)
4790 - Dr. J. Vomvoridis (JAYCOR)(50 copies)
4790 - Dr. H. Freund (SAI)

* Every name listed on distribution gets one copy except for those where extra copies are noted.

Dr. Tony Armstrong
SAI, Inc.
P. O. Box 2351
La Jolla, CA 92038

Dr. Robert Behringer
ONR
1030 E. Green
Pasadena, CA 91106

Dr. G. Bekefi (5 copies)
Massachusetts Institute of Technology
Bldg. 26
Cambridge, MA 02139

Dr. Arden Bement (2 copies)
Deputy Under Secretary of
Defense for R&AT
Room 3E114, The Pentagon
Washington, D.C. 20301

Dr. T. Berlincourt
Code 420
Office of Naval Research
Arlington, VA 22217

Dr. I. B. Bernstein (2 copies)
Yale University
Mason Laboratory
400 Temple Street
New Haven, CT 06520

Dr. Fred Burskirk
Physics Department
Naval Postgraduate School
Monterey, CA 93940

Dr. K. J. Button
Massachusetts Institute of Technology
Francis Bitter National Magnet
Laboratory
Cambridge, MA 02139

Dr. Gregory Canavan
Director, Office of Inertial Fusion
U. S. Department of Energy
M.S. C404
Washington, D.C. 20545

Dr. C. D. Cantrell
T-DOT, MS210
Los Alamos Scientific Laboratory
Los Alamos, NM 87545

Dr. Weng Chow
Optical Sciences Center
University of Arizona
Tucson, AZ 85721

Dr. Peter Clark
TRW, Building R-1, Room 1096
One Space Park
Redondo Beach, CA 90278

Dr. Robert Clark
P. O. Box 1925
Washington, D.C. 20013

Dr. William Colson
Quantum Institute
Univ. of California at Santa Barbara
Santa Barbara, CA 93106

Dr. William Condell
Code 421
Office of Naval Research
Arlington, VA 22217

Dr. Richard Cooper
Los Alamos Scientific Laboratory
P. O. Box 1663
Los Alamos, NM 87545

Cmdr. Robert Cronin
NFOIO Detachment, Suitland
4301 Suitland Road
Washington, D.C. 20390

Dr. R. Davidson (5 copies)
Plasma Fusion Center
Massachusetts Institute of Technology
Cambridge, MA 02139

Dr. John Dawson (2 copies)
Physics Department
University of California
Los Angeles, CA 90024

Defense Technical Information Center
(12 copies)
Cameron Station
5010 Duke Street
Alexandria, VA 22313

Dr. Francesco De Martini
Istituto de Fiscia
"G. Marconi" Univ.
Piazzo delle Science, 5
ROMA00185 ITALY

Prof. P. Diamant
Columbia University
Dept. of Electrical Engineering
New York, NY 10027

Prof. H. J. Doucet (5 copies)
Ecole Polytechnique
91128 Palaiseau
Paris, France

Dr. John Elgin (2 copies)
Imperial College
Dept. of Physics (Optics)
London SWF, England

Dr. David D. Elliott
SRI International
333 Ravenswood Avenue
Menlo Park, CA 94025

Dr. Norval Fortson
Department of Physics
University of Washington
Seattle, WA 98195

Director (2 copies)
National Security Agency
Fort Meade, MD 20755
ATTN: Mr. Richard Foss, A42

Dr. Robert Fossum, Director
(2 copies)
DARPA
1400 Wilson Boulevard
Arlington, VA 22209

Dr. Edward A. Frieman
Director, Office of Energy Research
U. S. Department of Energy
M.S. 6E084
Washington, D.C. 20585

Dr. George Gamota (3 copies)
OUSDRE (R&AT)
Room 3D1067, The Pentagon
Washington, D.C. 20301

Dr. Richard L. Garwin
IBM, T. J. Watson Research Center
P. O. Box 218
Yorktown Heights, NY 10598

Dr. Edward T. Gerry, President
W. J. Schafer Associates, Inc.
1901 N. Fort Myer Drive
Arlington, VA 22209

Dr. Avraham Gover
Tel Aviv University
Fac. of Engineering
Tel Aviv, ISRAEL

Dr. A. H. Guenter
Chief Scientist
Air Force Weapons Laboratory
Kirtland AFB, NM 87117

Mr. Donald L. Haas, Director
DARPA/STO
1400 Wilson Boulevard
Arlington, VA 22209

Dr. P. Hammerling
La Jolla Institute
P. O. Box 1434
La Jolla, CA 92038

Director
National Security Agency
Fort Meade, MD 20755
ATTN: Mr. Thomas Handel, A243

Dr. William Happer
560 Riverside Drive
New York City, NY 10027

Dr. Robert J. Hermann
Assistant Secretary of the
Air Force (RD&L)
Room 4E856, The Pentagon
Washington, D.C. 20330

Dr. Rod Hiddleston
KMS Fusion
Ann Arbor, MI 48106

Dr. J. L. Hirshfield (2 copies)
Yale University
Mason Laboratory
400 Temple Street
New Haven, CT 06520

Dr. R. Hofland
Aerospace Corp.
P. O. Box 92957
Los Angeles, CA 90009

Dr. Benjamin Huberman
Associate Director, OSTP
Room 476, Old Executive Office Bldg.
Washington, D.C. 20506

Dr. S. F. Jacobs
Optical Sciences Center
University of Arizona
Tucson, AZ 85721

Dr. Howard Jory (3 copies)
Varian Associates, Bldg. 1
611 Hansen Way
Palo Alto, CA 94303

Mr. Eugene Kopf
Principal Deputy Assistant
Secretary of the Air Force (RD&L)
Room 4E964, The Pentagon
Washington, D.C. 20330

Prof. N. M. Kroll
La Jolla Institutes
P. O. Box 1434
La Jolla, CA 92038

Dr. Tom Kuper
Optical Sciences Center
University of Arizona
Tucson, AZ 85721

Dr. Willis Lamb
Optical Sciences Center
University of Arizona
Tucson, AZ 85721

Mr. Mike Lavan
BMDATC-0
ATTN: ATC-0
P. O. Box 1500
Huntsville, AL 35807

Dr. John D. Lawson (2 copies)
Rutherford High Energy Lab
Chilton
Didcot, Oxon OX11 0OX
ENGLAND

Mr. Ray Leadabrand
SRI International
333 Ravenswood Avenue
Menlo Park, CA 94025

Mr. Barry Leven
NISC/Code 20
4301 Suitland Road
Washington, D.C. 20390

Dr. Donald M. LeVine (3 copies)
SRI International
1611 N. Kent Street
Arlington, VA 22209

Dr. Anthony T. Lin
University of California
Los Angeles, CA 90024

Director (2 copies)
National Security Agency
Fort Meade, MD 20755
ATTN: Mr. Robert Madden, R/SA

Dr. Joseph Mangano
DARPA
1400 Wilson Boulevard
Arlington, VA 22209

Dr. S. A. Mani
W. J. Schafer Associates, Inc.
10 Lakeside Office Park
Wakefield, MA 01880

Dr. Mike Mann
Hughes Aircraft Co.
Laser Systems Div.
Culver City, CA 90230

Dr. T. C. Marshall
Applied Physics Department
Columbia University
New York, NY 10027

Mr. John Meson
DARPA
1400 Wilson Boulevard
Arlington, VA 22209

Dr. Pierre Meystre
Projektgruppe fur Laserforschung
Max Planck Gesellschaft
Garching, Munich GERMANY

Dr. Gerald T. Moore
Optical Sciences Center
University of Arizona
Tucson, AZ 85721

Dr. Philip Morton
Stanford Linear Accelerator Center
P. O. Box 4349
Stanford, CA 94305

Dr. Jesper Munch
TRW
One Space Park
Redondo Beach, CA 90278

Dr. George Neil
TRW
One Space Park
Redondo Beach, CA 90278

Dr. Kelvin Neil
Lawrence Livermore Laboratory
Code L-321, P. O. Box 808
Livermore, CA 94550

Dr. Milton L. Noble (2 copies)
General Electric Company
G. E. Electronic Park
Syracuse, NY 13201

Prof. E. Ott (2 copies)
University of Maryland
Dept. of Physics
College Park, Md. 20742

Dr. Richard H. Pantell
Stanford University
Stanford, CA 94305

Dr. Richard M. Patrick
AVCO Everett Research Lab., Inc.
2385 Revere Beach Parkway
Everett, MA 02149

The Honorable William Perry
Under Secretary of Defense (R&E)
Office of the Secretary of Defense
Room 3E1006, The Pentagon
Washington, D.C. 20301

Dr. Alan Pike
DARPA/STO
1400 Wilson Boulevard
Arlington, VA 22209

Dr. Hersch Pilloff
Code 421
Office of Naval Research
Arlington, VA 22217

Dr. Charles Planner
Rutherford High Energy Lab
Chilton
Didcot, Oxon, OX11 0OX,
ENGLAND

Dr. Michal Poole
Daresbury Nuclear Physics Lab.
Daresbury, Warrington
Cheshire WA4 4AD
ENGLAND

Dr. Don Prosnitz
Lawrence Livermore Laboratory
Livermore, CA. 94550

Dr. D. A. Reilly
AVCO Everett Research Lab.
Everett, MA 02149

Dr. James P. Reilly
W. J. Schafer Associates, Inc.
10 Lakeside Office Park
Wakefield, MA 01880

Dr. A. Renieri
C.N.E.N.
Div. Nuove Attivita
Dentro di Frascati
Frascati, Rome
ITALY

Dr. Daniel N. Rogovin
SAI
P. O. Box 2351
La Jolla, CA 92038

Dr. Michael Rosenbluh
MIT - Magnet Lab.
Cambridge, MA 02139

Dr. Marshall N. Rosenbluth
Institute for Advanced Study
Princeton, NJ 08540

Dr. Eugene Ruane (2 copies)
P. O. Box 1925
Washington, D.C. 20013

Dr. Antonio Sanchez
MIT/Lincoln Laboratory
Room B231
P. O. Box 73
Lexington, MA 02173

Prof. S. P. Schlesinger
Columbia University
Dept. of Electrical Engineering
New York, NY 10027

Dr. Howard Schlossberg
APOSF
Bolling AFB
Washington, D.C. 20332

Dr. Stanley Schneider
Rotodyne Corporation
26628 Fond Du Lac Road
Palos Verdes Peninsula, CA 90274

Dr. Marlan O. Scully
Optical Sciences Center
University of Arizona
Tucson, AZ 85721

Dr. Robert Sepucha
DARPA/STO
1400 Wilson Boulevard
Arlington, VA 22209

Dr. A. M. Sessler
Lawrence Berkeley Laboratory
University of California
1 Cyclotron Road
Berkeley, CA 94720

Dr. Earl D. Shaw
Bell Labs
600 Mountain Avenue
Murray Hill, NJ 07974

Dr. Chan-Ching Shih
R&D Associates
P. O. Box 9695
Marina del Rey, CA 92091

Dr. Kenneth Smith
Physical Dynamics, Inc.
P. O. Box 556
La Jolla, CA 92038

Mr. Todd Smith
Hansen Labs
Stanford University
Stanford, CA 94305

Dr. Joel A. Snow
Senior Technical Advisor
Office of Energy Research
U. S. Department of Energy, M.S. E084
Washington, D.C. 20585

Mrs. Alma Spring
DARPA/Administration
1400 Wilson Boulevard
Arlington, VA 22209

SRI/MP Reports Area G037 (2 copies)
333 Ravenswood Avenue
Menlo Park, CA 94025
ATTN: D. Leitner

Dr. Abraham Szoke
Lawrence Livermore Laboratory
MS L-470, P. O. Box 808
Livermore, CA 94550

Dr. Milan Tekula
AVCO Everett Research Lab.
2385 Revere Beach Parkway
Everett, MA 02149

Dr. R. Temkin (2 copies)
Plasma Fusion Center
Massachusetts Institute of Technology
Cambridge, MA 02139

Dr. John E. Walsh
Department of Physics
Dartmouth College
Hanover, NH 03755

Dr. Wasneski (2 copies)
Naval Air Systems Command
Department of the Navy
Washington, D.C. 20350

Lt. Col. W. Whitaker
Defense Advanced Research Projects
Agency
1400 Wilson Boulevard
Arlington, VA 22209

Ms. Bettie Wilcox
Lawrence Livermore Laboratory
ATTN: Tech. Info. Dept. L-3
P. O. Box 808
Livermore, CA 94550

Dr. A. Yariv
California Institute of Tech.
Pasadena, CA 91125

Dr. T. Godlove
Department of Energy
Office of Laser Fusion
Germantown, MD 20545

Dr. A.W. Trivelpiece
Science Applications, Inc.
1200 Prospect St.
La Jolla, CA 92037

Dr. Jean Lebacqz
Stanford University
SLAC
Stanford, CA 94305

J.J. Tancredi
Hughes Aircraft Co.
Electron Dynamics Division
3100 Lomila Blvd.
Torrance, CA 90509

Dr. Paul Tallerico
Los Alamos Scientific Laboratory
P.O. Box 1663
Los Alamos, New Mexico 87545

Dr. M. Murphy (G-234)
Dept. of Energy
Washington, D.C. 20545

Dr. P. Stone (G-234)
Dept. of Energy
Washington, D.C. 20545

DATE
FILMED
8